An energy-efficient irregular hexagonal tessellation-based approach for connected *k*-coverage in planar wireless sensor networks

Kalyan Nakka, Habib M. Ammari[*]

Wireless Sensor and Mobile Autonomous Networks (WiSeMAN) Research Lab, Department of Electrical Engineering and Computer Science, Frank H. Dotterweich College of Engineering, Texas A&M University-Kingsville, Kingsville, TX 78363, USA

ARTICLE INFO

ABSTRACT

In the design of planar wireless sensor networks (PWSNs), the preliminary tasks are to achieve both coverage and connectivity, which are essential for the correct operation of this type of network. A PWSN is said to be in perfect operational condition only when it is capable of guaranteeing both coverage of the field and connectivity among all the active sensor nodes. In order to achieve both coverage and connectivity in PWSNs, we intend to solve the problem of connected *k*-coverage in PWSNs, where each point in a field of interest is covered (or sensed) by at least *k* sensor nodes ($k > 1$) simultaneously and all the participating sensor nodes in the *k*-coverage process are connected to each other. In our study, we found an irregular hexagon, denoted by $IrHx(r_s/n)$, as the best polygon for tessellating a field of interest and allowing to deploy sensor nodes, where $n > 1$ is a natural number and r_s is the radius of the sensing range of the sensor nodes. First, we construct our proposed irregular hexagon, $IrHx(r_s/n)$, which forms a tile, using the regular hexagon. Second, we compute the minimum sensor density required to *k*-cover a planar field of interest using our proposed $IrHx(r_s/n)$ tile. Third, we establish a relationship between the sensing and communication radii of the sensor nodes to ensure network connectivity in *k*-covered PWSNs. Finally, we substantiate our theory with various simulation results.

1. Introduction

Planar wireless sensor networks (PWSNs) are infrastructure-less and wirelessly connected networks that are formed by the deployment of tiny, standalone battery-powered sensor nodes in a field of interest along with a central entity, called *sink*, to which all the sensor nodes relay the gathered data for further analysis and processing. Sensor nodes (or simply *sensors*) gather information using their sensing capabilities and transmit the information to the sink using their communication capabilities. Therefore, in order to ensure successful data collection and transmission during the network operation, it is important that PWSNs make certain that both coverage and connectivity are guaranteed throughout the network operational lifetime.

This requirement of consistency for coverage and connectivity constrains the deployment of sensors in a planar field of interest such that there are no coverage or connectivity gaps in PWSNs. Moreover, for crucial applications of PWSNs, such as intruder detection and tracking, multi-coverage (or redundant coverage) of a point in a planar field by the sensors is necessary. This concept of multi-coverage ensures fault-tolerant data collection. In this paper, we focus on a more general

concept of such multi-coverage, called planar *k*-coverage, where every point in a planar field of interest is covered by at least *k* sensors at the same time. We attempt to solve the connected *k*-coverage problem in PWSNs, where *k*-coverage along with network connectivity are ensured. In the following section, we elaborate this problem further (Section 1.1). Then, we highlight our contributions in this paper (Section 1.2).

1.1. Problem statement

We want to investigate the connected *k*-coverage problem in PWSNs, where every point in a field of interest is covered (or sensed) by at least *k* sensors simultaneously, while all the underlying sensors are mutually connected to each other so that there is at least one communication path between any pair of sensors, where $k > 1$ is the requested coverage degree. Additionally, the connected *k*-coverage problem can be partitioned into four major inter-connected sub-problems, which we aim to answer thoroughly. These four sub-problems, can be formulated as follows:

- **Sub-problem 1:** What is the optimal sensor deployment strategy so that every point in a planar field of interest is sensed by at least k sensors simultaneously, while using a minimum set of sensors, where $k > 1$ is a natural number designating the coverage degree?
- **Sub-problem 2:** What is the minimum planar sensor density (i.e., number of sensors per unit area) to ensure k-coverage of a planar field according to the strategy formulated in Sub-problem 1 above?
- **Sub-problem 3:** What is the necessary constraint between the sensing and communication radii of the sensors that ensures network connectivity?
- **Sub-problem 4:** How should the sensors be selected and scheduled (or duty-cycled) to k-cover a planar field using a deployed sensor density that is as close as possible to the theoretical one, which is computed in solving Sub-problem 2 above?

1.2. Contributions and organization

We consider the concept of tessellating a field of interest and deploying the sensors using to tiles generated by this tessellation such that connected k-coverage in PWSNs is achieved using a minimum set of sensors. The major contributions of this paper can be summarized as follows:

- We tesselate the field of interest using regular hexagon, with specific constraints. Based on this tessellation, we propose a sensor deployment strategy for 1-coverage (or simply coverage), and calculate the corresponding planar sensor density.
- We extend the above-mentioned 1-coverage approach to k-coverage by (1) creating an irregular hexagon, which modifies the size of the tile of the tessellation configuration created earlier, and (2) placing k sensors in each tile to achieve k-coverage of a planar field. Based on this irregular hexagon, we compute the corresponding planar sensor density for k-coverage, and derive a general irregular hexagon $IrHx$ (r_s/n), where r_s is the radius of the sensing range of the sensors and $n > 1$.
- We establish the relationship between the sensing and communication radii of the sensors for the previously proposed sensor deployment strategy using the irregular hexagon, $IrHx(r_s/n)$. This relationship is a necessary constraint that ensures that all the sensors involved in the k-coverage process are mutually connected, thus, achieving connected k-coverage in PWSNs, where $k > 1$.
- We propose an optimal sensor selection protocol that selects a minimum set of sensors to k-cover a planar field. This protocol helps ensure optimal energy dissipation per sensor, which in turn helps extend the operational network lifetime.

The remainder of this paper is structured as follows. Section 2 discusses the existing research on the problem of k-coverage in PWSNs. Section 3 presents some fundamental concepts and introduces the network and energy models used in our investigation of the connected k-coverage problem in PWSNs. Section 4 focuses on the study of 1-coverage using the regular hexagonal tessellation, and its extension to solve the k-coverage problem by constructing an irregular hexagon $IrHx$ (r_s/n), whose side length is proportional to the ratio r_s/n, where r_s stands for the radius of the sensing range of the sensors and n is a natural number with $n > 1$, using a diamond-shaped area based on the existing regular hexagonal tessellation, and deploying k sensors in it to achieve k-coverage. In addition, using this generalized irregular hexagon, $IrHx(r_s/n)$, we establish the necessary condition for ensuring network connectivity of all the sensors participating in the k-coverage process in PWSNs. Section 5 discusses our proposed connected k-coverage protocol, called k-InDi. Section 6 presents our simulation results for evaluating our connected k-coverage protocol, k-InDi, and compare them with those of our theoretical analysis. Furthermore, we compare the performance of our protocol, k-InDi, with that of an existing connected k-coverage protocol, called RCH$_k$ [11]. Section 7 concludes this paper and discusses

possible future directions and extensions of our proposed work.

2. Related work

In this section, we briefly discuss various approaches for solving the coverage and k-coverage problem in planar wireless sensor networks. Moreover, these solutions are discussed briefly along with their limitations compared to our approach.

2.1. Literature review

Wang et al. [5,6] formulated an algorithm for k-coverage eligibility which toggles a sensor state (active or inactive) by evaluating the coverage of intersection points of sensing ranges of that sensor with its neighboring sensors and proposed a coverage configuration protocol (CCP). Ammari has leveraged the geometrical properties of Reuleaux triangle and developed a connected k-coverage theory using Reuleaux triangle-based tessellation, such that connected k-coverage is attained through the sensor placement strategy of positioning k sensors in the lens formed between two Reuleaux triangles. Based on this theory, Ammari has developed various protocols for PWSNs such as stochastic protocol SCP$_k$ [7], randomized protocols CERACC$_k$ and DIRACC$_k$ [8], clustering-based protocols T-CRACC$_k$ and D-CRACC$_k$ [8] and heterogeneous protocols PR-Het-CCC$_k$ and PR-Het-DCC$_k$ [10]. Yu et al. [12] developed a k-coverage theory using regular pentagons where each sensor's sensing range is modelled using four regular pentagons with central areas and k-coverage is attained if there are k-1 sensors collectively in those four central areas. Yu et al. [14] has leveraged Ammari's [7–10] k-coverage theory for constructing coverage contribution area (CCA) for sensor placement using Reuleaux triangle-based tessellation, and proposed SCRT-PCA$_k$, DCRT-PCA$_k$ and DIRT-PCA$_k$ protocols.

Qiu et al. [13] has achieved k-coverage by creating k-order local k-coverage Voronoi diagram (LVD), which allocates neighboring sensors to an under k-covered sensor for achieving the degree of coverage k, and also to precision check the critical points for any sensor. In order to address the coverage void problem that may arise and simultaneously attain k-coverage, they proposed distributed Voronoi-based cooperation (DVOC) scheme that uses both k-order LVDs and k-order Delaunay triangles. Sun et al. [15] addressed the k-coverage problem using the process of optimization node deployment. Abbasi et al. [16] proposed a coverage control method for continuous and potentially long regions and passages, where a group of autonomous mobile sensors move within the region/passage boundaries for maintaining optimal coverage. Qin and Chen [20] proposed an area coverage algorithm for achieving the coverage demand that uses the binary differential evolution (DE) for searching an improved subset of nodes in the network, which ensures specific coverage ratio. Chenait et al. [17] has developed sector redundancy determination algorithm which uses a predefined angle for slicing the sensing range of sensor and also determines the redundant sensors for k-coverage process, and proposed SRA-Per and SRA-SP protocols. Krishnan et al. [21] leveraged four different optimization schemes, namely heuristic algorithm, ABC algorithm, ant colony optimization (ACO) algorithm and particle swarm optimization (PSO) algorithm, for the determination of sensor placement positions, and used minimum dominating set-based heuristics for sensor scheduling. Using various combinations of these sensor placement and sensor scheduling schemes, they proposed ten protocols and studied their performance.

Elhoseny et al. [22] utilized genetic algorithm-based (GA) approach, with an objective of maximizing the network operational lifetime, for achieving k-coverage of target locations in the field of interest. Hoyingcharoen and Teerapabkajorndet [18] developed theory for determining the expected sensing probability of any location and computing the expected connectivity level of any sensor to sink. Based on this theory, they demonstrated its capabilities in predicting connectivity and coverage levels. Naik and Shetty [23] also leveraged the DE algorithm for evaluating the field of interest and determining the

Table 1
Comparison with existing research.

Research Problem	Studies	Contribution of our approach
target coverage	[20,21,26]	**Contribution 1**: Ensures fault-tolerant sensor data collection with zero coverage holes by achieving *k*-coverage of field of interest, and, **Contribution 2**: Ensures reliable connectivity of sensors with zero connectivity holes due to our *k*-coverage theory's network connectivity relationship
target *k*-coverage	[21,22, 26–28]	**Contribution 2** and, **Contribution 3**: Ensures reliable monitoring of the field of interest by achieving *k*-coverage of each and every point/location of the field of interest.
target *k*-coverage and *m*-connectivity	[23–25]	**Contribution 2, Contribution 3** and, **Contribution 4**: Ensures reliable data transmission between sensors and sink by achieving connectivity of all active sensors involved in the *k*-coverage process.
k-coverage	[12,13,15, 19]	**Contribution 5**: Ensures reliable connectivity of sensors with zero connectivity holes due to our *k*-coverage theory's network connectivity relationship, and, **Contribution 6**: Ensures longer network lifetime due to use of minimal number of active sensors for *k*-coverage due to the tessellation.
connected *k*-coverage (geometry-based)	[5,6,17]	**Contribution 6** and, **Contribution 7**: Ensures reliable network connectivity with low-powered sensors due to our *k*-coverage theory's network connectivity relationship.
connected *k*-coverage (tessellation-based)	[7,8,10,11, 14,31,32]	**Contribution 6**, **Contribution 8**: Ensures use of lesser number of active sensors for *k*-coverage due to lower planar sensor density, and, **Contribution 9**: Ensures lesser energy consumption per *k*-coverage round due to lower planar sensor density.

candidate locations for optimal sensor placement in order to attain *k*-coverage of target locations in the field of interest. Tarnaris et al. [26] have also addressed both the problems of area coverage and *k*-coverage of target locations using PSO and GA algorithms. Harizan and Kuila [24] proposed *k*-coverage solutions inspired by heuristic and nature-inspired algorithms, where *k*-coverage of target locations in the field of interest is achieved by placing the sensors at specific optimal locations. These optimal locations are determined using GA, PSO, DE and gravitational search algorithms. Natarajan and Parthiban [25] have leveraged shuffled frog leaping Nelder-Mead algorithm for determining optimal node positions such that *k*-coverage of specific target locations is achieved.

Torshizi and Sheikhzadeh [19] have proposed a distributed algorithm CLARRKC, which leverages Cellular Learning Automata (CLA) for sleep scheduling of sensors such that *k*-coverage is achieved with optimal number of sensors by removing redundant active sensors from *k*-coverage operation. Ammari [11] has suggested that regular hexagon is the best regular polygon for modeling the sensing range of a sensor. He exploited regular hexagon-based tessellation for achieving *k*-coverage by placing the sensors in sliced hexagons and proposed *k*-coverage algorithm RCH$_k$, that works for any sensing model as well as any configuration of PWSNs. Alibeiki et al. [27] has addressed the problem of *k*-coverage in directional PWSNs, for both over-provisioned and under-provisioned sensor configurations using GA-based approach. Elloumi et al. [28] have proposed two solutions by formulating the target *k*-coverage problem with mixed linear programming of Single commodity flow model and Miller-Tucker-Zemlin model. Nakka et al. [31,32] constructed cusp square-based square tessellation for achieving

connected *k*-coverage and proposed centralized protocol *k*-CSqu [31], which is better than DIRACC$_k$ [8], and stochastic protocol St-*k*-CSqu [32], which is better than SCP$_k$ [7].

2.2. Discussion

In [13], DVOC uses *k*-order LVDs for achieving *k*-coverage whereas we use regular convex polygonal tessellation for *k*-coverage, in this paper it is irregular hexagon-based. In addition DVOC [13] utilizes *k*-order Delaunay triangles for the mitigation of existing or newly generated coverage voids that are generated by *k*-order LVDs, whereas in our research, there are zero coverage voids due to *k*-coverage of each tile of the tessellation. It is observed that the *k*-coverage research studies using computational intelligence algorithms [20–27] use optimal number of sensors, improving the operational network lifetime. But the limitation of these approaches is that they can be employed for *k*-covering specific target locations in the field of interest, whereas our approach will ensure *k*-coverage of each and every point/location of the entire field of interest. Moreover, connectivity of all active sensors and avoiding connectivity holes is still a challenge for most of the approaches discussed [19–28], whereas our approach maintains connectivity of all active sensors in the network as well as zero connectivity holes. It is worth noting that unlike our approach, except tessellation based research [7–12,14,31], none of the other solutions could quantitatively estimate minimum sensor density required for *k*-coverage of the field of interest in PWSNs. Table 1 describes the contributing areas of our approach in-comparison with existing research, discussed in the previous section.

Compared to tessellation-based research [7–11,14,31], in this paper's proposed approach, geometric properties of irregular hexagon are leveraged for attaining *k*-coverage in PWSNs. Furthermore, our irregular hexagon tessellation approach, discussed in further sections, outperforms all tessellation-based research [7–11,14,31] in terms of planar sensor density, number of active sensors for *k*-coverage and operational network lifetime of PWSNs, making our approach more energy-efficient than these existing approaches [7–11,14,31].

3. Preliminaries and models

In this section, we introduce the terminology used in this paper. Also, we describe our network and energy models along with their assumptions, which are used in formulating our solution to the connected *k*-coverage problem in PWSNs.

3.1. Terminology

Definition 1 (*Sensing range*) – The *Sensing range* of a sensor *s* is its surrounding area A_S, such that *s* can detect any event occurring in A_S.

Definition 2 (*Communication range*) – The *Communication range* of a sensor *s* is its surrounding area A_C, such that *s* can communicate with any sensor located in A_C.

Definition 3 (*k-Coverage*) – A field *F* is said to be *k*-covered if every point of *F* is covered by at least *k* sensors simultaneously, where $k > 1$. The underlying PWSN is said to ensure *k*-coverage of the field *F*.

Definition 4 (*Connected k-coverage*) – A PWSN is said to be guaranteeing *connected k-coverage* if ensures *k*-coverage, where all the sensors involved in the *k*-coverage process are mutually connected, thus, facilitating at least one communication path, whether direct or indirect, between any pair of sensors.

Definition 5 (*Planar sensor density*) – The *planar sensor density* of PWSNs monitoring a field of interest *F* is the number of sensors per unit area required to *k*-cover *F*.

Definition 6 (*Polygonal Tessellation*) – A *polygonal tessellation* of a field of interest *F* consists overlaying *F* by adjacent and non-intersecting copies of a polygonal shape without causing any gaps.

Definition 7 (*Tile*) – A *tile* is a convex polygonal shape that can generate a polygonal tessellation of a field of interest.

3.2. Network model

Assumption 1 (*Homogeneous Sensors*): All the sensors of PWSNs have the same characteristics, including their initial energy reserves, sensing range, and communication range.

Assumption 2 (*Random and Uniform Deployment*): All the sensors are randomly and uniformly deployed in a planar field of interest with specific sensor density ρ.

Assumption 3 (*Location Awareness*): Every sensor has knowledge of its location via a global positioning system (GPS) or any localization technique [1]

Assumption 4 (*Disk Model*): Both of the sensing and communication ranges of the sensors follow the disk model. That is, they are represented by disks of radii r_s and r_c, respectively, whose centers coincide with location of the corresponding sensor.

Assumption 5 (*Sensor Mobility*): All the sensors are mobile and can freely move to specific locations in the field of interest.

3.3. Energy model

We have used the energy model suggested by Heizelman et al. [2] for computing the energy consumed by the sensors, while performing the activities of data transmission and data reception.

$$E_t(d) = b \times (\varepsilon d^\alpha + E_e) \quad E_r = b \times E_e$$

where $E_t(d)$ is the energy consumed by sensor s for transmitting a message of b bits over a distance d, E_r is the energy spent by sensor s for receiving a message of size b bits, E_e is the electronical energy, $\varepsilon \in \{\varepsilon_{fs}, \varepsilon_{mp}\}$ is the transmitter amplifier in the free space (ε_{fs}) or multi-path (ε_{mp}) model, and $\alpha \in [2,4]$ is the exponent of path-loss.

The energy consumed by the sensors for performing the sensing tasks is estimated based on the energy model proposed by Ye et al. [3]In an ideal scenario, a sensor utilizes 0.012 J of energy (E_{idle}) in idle mode, 0.0003 J of energy (E_{sleep}) in sleep mode, and the energy consumed for sensor movement (E_{move}) is randomly picked from the range [0.008, 0.012] J/m [4]

3.4. Lifetime model

In this work, we define the network lifetime as the length of time from the deployment of network till the last sensor of network runs out of energy. The lifetime of the deployed PWSN can be evaluated as,

$$\mathscr{L} = \frac{E_{init}^N}{E_{consume}^k}$$

where E_{init}^N is total initial energy (or) battery power of the entire PWSN and $E_{consume}^k$ is total energy (or) battery power consumption of all active sensors participating in k-coverage process.

4. Hexagonal tessellation for k-coverage

In this section, we investigate the problem of k-covering a planar field using hexagonal tiles. Next, we state our instance of the planar k-coverage problem as follows:

Instance of the k-coverage problem: For a given set of sensors and a hexagonal tessellation of a planar field, what is the best sensor deployment strategy for achieving k-coverage of that field, where every hexagonal tile of the tessellation can be k-covered by at least k sensors, where $k > 1$ is the degree of coverage?

In order to investigate the k-coverage problem stated above, we are interested in solving the 1-coverage problem of PWSNs, where every
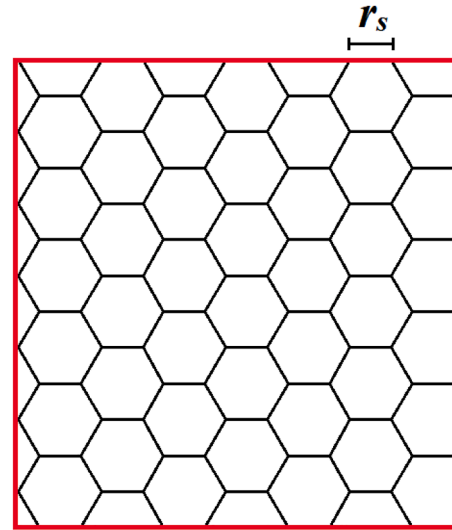

Fig. 1. Regular hexagonal tessellation with side length r_s.

point in a planar field is covered by at least 1 sensor based on a hexagonal tessellation of this field.

4.1. Regular hexagon-based tessellation

We consider the regular hexagon as the tile of side length r_s [11] for tessellating a planar field, where r_s is the radius of sensing range of the sensors. First, we specify the sensor deployment strategy for attaining 1-coverage in PWSNs.

Sensor deployment for 1-coverage: As mentioned earlier, we tessellate a planar field using regular hexagons of side r_s, as shown in Fig. 1. We place one sensor at the center of each regular hexagonal tile to achieve 1-coverage in PWSN.

Planar sensor density for 1-coverage: To achieve 1-coverage of a planar field, the corresponding planar sensor density for the above sensor deployment strategy and regular hexagon tessellation, is given by:

$$\lambda(r_s) = \frac{1}{A_{SR}} = \frac{1}{\pi r_s^2} = \frac{0.318}{r_s^2}$$

We can easily determine that the farthest distance between any two neighboring sensors is $\sqrt{3}r_s$. Therefore, for any 1-coverage configuration, network connectivity is ensured if the following inequality between the sensing and communication radii of the sensors, r_c and r_s, respectively, holds:

$$r_c \geq \sqrt{3}r_s$$

In order to extend this sensor deployment strategy to address the k-coverage problem, we have to place k sensors at the center of each regular hexagonal tile. However, placing k sensors at the center of every regular hexagonal tile is unrealistic and not possible in real-world scenarios. Thus, in order to place k sensors, it is more realistic to have a dedicated area in every tile.

4.2. Construction of irregular hexagonal tile

First, we modify the regular hexagon tessellation by setting its side length to $r_s/2$. Second, we consider a diamond area formed by two equilateral triangles of same base in the tessellation for placing k sensors (solution to sub-problem 1 in 1.1), and construct an irregular hexagon, which can be used as tile for tessellating a planar field of interest.

Let us consider a diamond area, denoted by D, of the tessellation. We draw circles of radius r_s centered at each vertex of D, where an enclosed area is formed by the intersection of these four circles. In the intersection
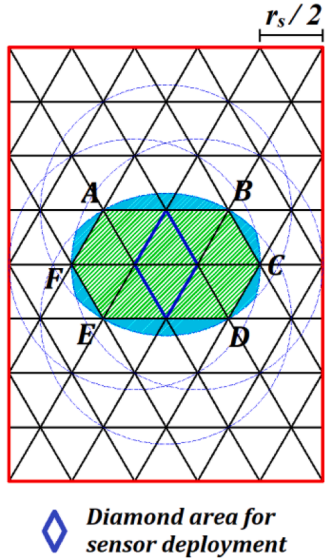
Fig. 2. Construction of the irregular hexagon $IrHx(r_s/2)$.

4.3. Generalized irregular hexagonal tile

We observed that the planar sensor density $\lambda(k, r_s)$ corresponding to our irregular hexagon-based configuration is not only dependent on number of sensors k and the radius r_s of the sensing range of the sensors, but also on side length of the regular hexagonal tessellation, which is proportional to the sensing radius r_s. Let us consider a more generic side length of r_s/n for our regular hexagonal tessellation so as to understand the properties of our generalized irregular hexagon, denoted by $IrHx(r_s/n)$. As noted from our previous cases ($n = 2, 3, 4$ and 5), our generalized irregular hexagon $IrHx(r_s/n)$ has a certain structure in terms of the lengths of each of the six sides, i.e., $\overline{AB}, \overline{BC}, \overline{CD}, \overline{DE}, \overline{EF}$ and $\overline{FA}$, the number of rings of equilateral triangles comprising it, and the number of triangles per ring as shown with different colors in Fig. 3. Table 2(a) demonstrates the structure of our generalized irregular hexagon $IrHx(r_s/n)$, and Table 2(b) shows the number of equilateral triangles per ring, both for $n = 2, 3, 4, 5$.

Using Table 2(a) given above, we extend those results to our generalized irregular hexagon $IrHx(r_s/n)$, where the side length of the equilateral triangle is r_s/n. Table 3 illustrates those generic results for $IrHx(r_s/n)$.

Lemma 1 below, which exploits the results illustrated in Table 3, computes the number of equilateral triangles for any ring l of our generalized irregular hexagon $IrHx(r_s/n)$.

Lemma 1. *(Number of triangles per ring): In a generalized irregular hexagon IrHx(r$_s$/n), the number of equilateral triangles in ring l, denoted by N$_l$, can be computed as:*

$$N_l = 12l - 2$$

area, we obtain an irregular hexagon, denoted by $IrHx(r_s/2)$, which is formed by 10 equilateral triangles of side length $r_s/2$, as shown in Fig. 2. This irregular hexagon $IrHx(r_s/2)$ can be used as a tile to tessellate a planar field of interest.

The coverage A_k for the configuration shown in Fig. 2 is the sum of all 10 equilateral triangle areas and all curvature areas formed at each side of the irregular hexagon. This area A_k is computed as follows:

$$A_k = \left[\pi + \frac{\sqrt{3}}{8} - \frac{\sqrt{15}}{4} - 4 \sin^{-1}\left(\frac{1}{4}\right) \right] r_s^2 = 1.3791 r_s^2$$

Thus, the corresponding planar sensor density for the above irregular hexagon-based sensor deployment can be calculated as follows:

$$\lambda(k, r_s) = \frac{k}{A_k} = \frac{k}{1.3791 r_s^2} = \frac{0.7251\, k}{r_s^2}$$

Similarly, we can generate $IrHx(r_s/3)$, $IrHx(r_s/4)$ and $IrHx(r_s/5)$, by modifying the side length of the regular hexagonal tessellation as $r_s/3$, $r_s/4$, and $r_s/5$, respectively, as shown in Fig. 3. We found that the planar sensor density $\lambda(k, r_s)$ pertaining to our irregular hexagon $IrHx(r_s/3)$ is lesser than that of $IrHx(r_s/2)$. Likewise, we found that the results achieved by $IrHx(r_s/4)$ are better than those related to $IrHx(r_s/3)$, and the results obtained for $IrHx(r_s/5)$ are better than those generated by $IrHx(r_s/4)$.
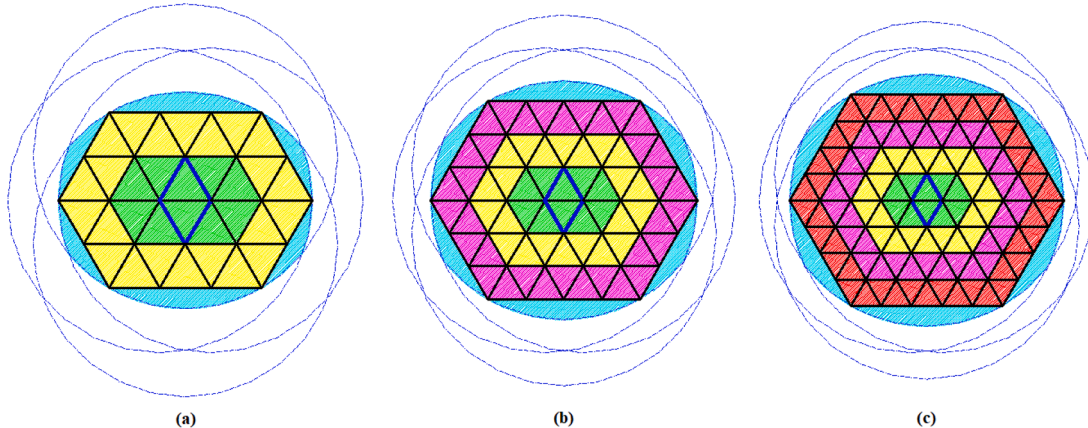
Table 2a
$IrHx(r_s/n)$ structure for n.

n	$\overline{AB}$	$\overline{BC}$	$\overline{CD}$	$\overline{DE}$	$\overline{EF}$	$\overline{FA}$	# Rings
2	r_s	$r_s/2$	$r_s/2$	r_s	$r_s/2$	$r_s/2$	1
3	r_s	$2r_s/3$	$2r_s/3$	r_s	$2r_s/3$	$2r_s/3$	2
4	r_s	$3r_s/4$	$3r_s/4$	r_s	$3r_s/4$	$3r_s/4$	3
5	r_s	$4r_s/5$	$4r_s/5$	r_s	$4r_s/5$	$4r_s/5$	4

Table 2b
Number of triangles per ring of $IrHx(r_s/n)$ for n.

n	Ring #1	Ring #2	Ring #3	Ring #4
2	10			
3	10	22		
4	10	22	34	
5	10	22	34	46

Fig. 3. Irregular hexagons of side length (a) $r_s/3$, (b) $r_s/4$, and (c) $r_s/5$.

Table 3
Generic structure of $IrHx(r_s/n)$.

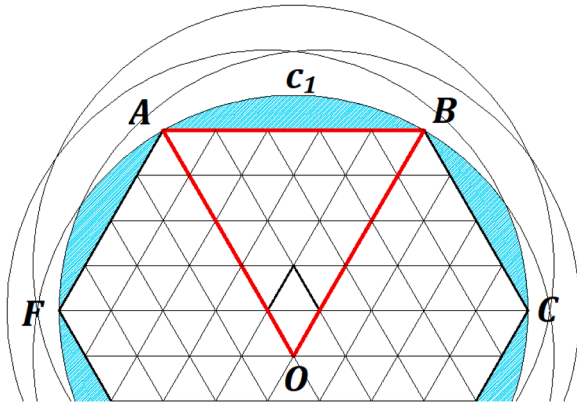|	$\overline{BC}$	$\overline{CD}$	$\overline{DE}$	$\overline{EF}$	$\overline{FA}$	# Rings
r_s	$\dfrac{(n-1)r_s}{n}$	$\dfrac{(n-1)r_s}{n}$	r_s	$\dfrac{(n-1)r_s}{n}$	$\dfrac{(n-1)r_s}{n}$	$n-1$

Fig. 4. Curved area between arc AB and line segment AB.

Proof: The results of Table 2(b) illustrate that for any value of n, the number of triangles for a certain ring of $IrHx(r_s/n)$ is constant, i.e., for a ring p, the number of equilateral triangles $N_{l=p}$ is same for all values of n, where n is natural number and $n > 1$. Let us consider the results in Table 2(b) for $n = 5$, we have $N_{l=1} = 10$, $N_{l=2} = 22$, $N_{l=3} = 34$, and $N_{l=4} = 46$. It is clear that the difference between the consecutive pairs of N_l values is constant, i.e., $N_{l=2} - N_{l=1} = N_{l=3} - N_{l=2} = N_{l=4} - N_{l=3} = 12$. Thus, we can say that the N_l values for all rings of our generalized irregular hexagon are in arithmetic progression (or sequence), where the initial term $N_0 = 10$ and common difference $d = 12$. This means that l^{th} term of this arithmetic progression gives us the number of equilateral triangles present in the ring l. Therefore, number of equilateral triangles in ring l is computed as:

$$N_l = 10 + (l-1) \times 12 = 12l - 2$$

Lemma 2 below computes the total number of equilateral triangles in our generalized irregular hexagon $IrHx(r_s/n)$, by leveraging the results of Lemma 1.

Lemma 2. *(Total Number of Triangles in $IrHx(r_s/n)$: Total number of equilateral triangles N, which comprise our generalized irregular hexagon $IrHx(r_s/n)$, is given by:*

$$N = 2(n-1)(3n-1)$$

Proof: From Lemma 1, we know that the number of equilateral triangles for any ring l of our generalized irregular hexagon $IrHx(r_s/n)$ is $N_l = 12l - 2$, and the total number of its rings is $n - 1$. Therefore, the total number N of equilateral triangles of $IrHx(r_s/n)$ can be calculated as follows:

$$N = \sum_{l=1}^{n-1} N_l = \sum_{l=1}^{n-1} 12l - 2 = \sum_{l=1}^{n-1} 12l - \sum_{l=1}^{n-1} 2 = 12 \times \sum_{l=1}^{n-1} l - 2 \times \sum_{l=1}^{n-1} 1$$

$$\Rightarrow N = 12 \times \frac{(n-1)n}{2} - 2 \times (n-1) = 6n(n-1) - 2(n-1) = 2(n-1)(3n-1)$$

Therefore, total number of equilateral triangles of $IrHx(r_s/n)$ is given by $N = 2(n-1)(3n-1)$

Lemma 3 below computes the size of the curved area between the arc AB and line segment $\overline{AB}$, which is also the same curved area between the
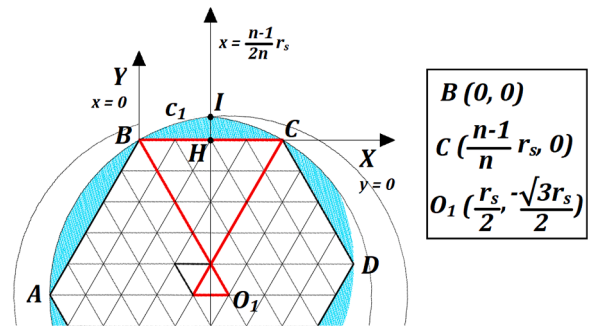

Fig. 5. Curved area formed above the line segment BC.

arc DE and line segment $\overline{DE}$.

Lemma 3. *(Size of Curved Area Above Longer Side): The size A_{LS} of the curved area suspended between the arc AB and line segment $\overline{AB}$ (i.e., curved area above the longer side) is computed as follows:*

$$A_{LS} = \left(\frac{\pi}{6} - \frac{\sqrt{3}}{4} \right) r_s^2$$

where r_s is the radius of the sensing range of the sensors.

Proof: From Fig. 4, it is evident that the circle c_1 passing through the vertices A and B is centered at vertex O. Therefore, the size of the curved area formed between the arc AB and line segment $\overline{AB}$ is given by:

$$A_{LS} = A_{Sector\ AOB} - A_{Triangle\ AOB} = \frac{\pi r_s^2}{6} - \frac{\sqrt{3} r_s^2}{4} = \left(\frac{\pi}{6} - \frac{\sqrt{3}}{4} \right) r_s^2$$

Lemma 4 below computes the size of the curved area formed above the line segment $\overline{BC}$, which is formed by the intersection of two circles. It is worth noting that the curved areas formed above the sides $\overline{BC}$, $\overline{CD}$, $\overline{EF}$, and $\overline{FA}$ are all equal.

Lemma 4. *(Size of Curved Area Above Shorter Side): The size A_{SS} of the curved area formed above the side $\overline{BC}$ (i.e., curved area above the shorter side) is computed as follows:*

$$A_{SS} = \left[\frac{\pi}{6} + \sin^{-1}\left(\frac{-1}{2n} \right) - \frac{\sqrt{4n^2 - 1}}{4n^2} - \frac{\sqrt{3}(n-2)}{4n} \right] r_s^2$$

where r_s stands for the radius of the sensing range of the sensors.

Proof: Let us consider the coordinate system shown in Fig. 5, where the side BC is X-axis and B is the origin. It is evident that the area suspended by the arc BI and the line segment BH is equal to the area suspended by the arc CI and the line segment CH, due to symmetry, where vertex I is the intersection point of two circles and H is the mid-point of the side $\overline{BC}$. As the circle c_1 is centered at vertex $O_1 \left(\frac{r_s}{2}, \frac{-\sqrt{3}r_s}{2} \right)$, we have the following equation of the circle c_1:

$$c_1: \left(x - \frac{r_s}{2} \right)^2 + \left(y + \frac{\sqrt{3}r_s}{2} \right)^2 = r_s^2$$

$$\Rightarrow y_{c_1} = \sqrt{r_s^2 - \left(x - \frac{r_s}{2} \right)^2} - \frac{\sqrt{3}r_s}{2}$$

Now, we can compute the size A_{BIH} of the area between the arc BI and line segment BH as follows:

$$A_{BIH} = \int_0^{\frac{n-1}{2n}r_s} \int_0^{y_{c_1}} dy\, dx = \int_0^{\frac{n-1}{2n}r_s} y_{c_1}\, dx = \int_0^{\frac{n-1}{2n}r_s} \sqrt{r_s^2 - \left(x - \frac{r_s}{2}\right)^2} - \frac{\sqrt{3}r_s}{2}\, dx$$

$$\Rightarrow A_{BIH} = \left[\frac{\pi}{6} + \sin^{-1}\left(\frac{-1}{2n}\right) - \frac{\sqrt{4n^2-1}}{4n^2} - \frac{\sqrt{3}(n-2)}{4n}\right]\frac{r_s^2}{2}$$

Therefore, the size A_{SS} of the curved area formed above the side $\overline{BC}$ is given by:

$$A_{SS} = 2 \times A_{BIH}$$

$$\Rightarrow A_{SS} = \left[\frac{\pi}{6} + \sin^{-1}\left(\frac{-1}{2n}\right) - \frac{\sqrt{4n^2-1}}{4n^2} - \frac{\sqrt{3}(n-2)}{4n}\right]r_s^2$$

Lemma 5 below computes the size of a k-covered area based on our generalized irregular hexagon $IrHx(r_s/n)$. It exploits the results stated in Lemma 2, Lemma 3, and Lemma 4.

Lemma 5. *(k-Covered Area): The size A_k of a k-covered area that is formed by the intersection of the sensing disks of k sensors, which are placed in the inner diamond area of our generalized irregular hexagon $IrHx(r_s/n)$, can be computed as follows:*

$$A_k = \left[\pi + \frac{(3n^2-6n+2)\sqrt{3}}{4n^2} - \frac{\sqrt{4n^2-1}}{n^2} - 4\sin^{-1}\left(\frac{1}{2n}\right)\right]r_s^2$$

where r_s is the radius of the sensing range of the sensors, and n is a natural number such that $n \geq 1$.

Proof: The k-covered area is the largest area of the intersection region formed by the sensing disks of the sensors that are placed at the vertices of the inner diamond area of our generalized irregular hexagon $IrHx(r_s/ n)$. The size A_k of this k-covered area is given by:

$$A_k = A_{Hexagon\ ABCDEF} + A_{Curved\ area\ above\ AB} + A_{Curved\ area\ above\ BC}$$
$$+ A_{Curved\ area\ above\ CD} + A_{Curved\ area\ above\ DE} + A_{Curved\ area\ above\ EF}$$
$$+ A_{Curved\ area\ above\ FA}$$

Notice that we have:

$$A_{Hexagon\ ABCDEF} = N \times \frac{\sqrt{3}}{4}\left(\frac{r_s}{n}\right)^2 = (n-1)(3n-1)\frac{\sqrt{3}}{2}\left(\frac{r_s}{n}\right)^2 \text{ (Lemma 2),}$$

$A_{Curved\ area\ above\ AB} = A_{Curved\ area\ above\ DE} = A_{LS}$ (Lemma 3) and,

$A_{Curved\ area\ above\ BC} = A_{Curved\ area\ above\ CD} = A_{Curved\ area\ above\ EF} = A_{Curved\ area\ above\ FA} = A_{SS}$ (Lemma 4)

Finally, A_k can be computed as follows:

$$A_k = A_{Hexagon\ ABCDEF} + 2A_{LS} + 4A_{SS}$$

$$= (n-1)(3n-1)\frac{\sqrt{3}}{2}\left(\frac{r_s}{n}\right)^2 + 2 \times \left(\frac{\pi}{6} - \frac{\sqrt{3}}{4}\right)r_s^2 + 4$$

$$\times \left[\frac{\pi}{6} + \sin^{-1}\left(\frac{-1}{2n}\right) - \frac{\sqrt{4n^2-1}}{4n^2} - \frac{\sqrt{3}(n-2)}{4n}\right]r_s^2$$

$$= \left[\pi + \frac{(3n^2-6n+2)\sqrt{3}}{4n^2} - \frac{\sqrt{4n^2-1}}{n^2} - 4\sin^{-1}\left(\frac{1}{2n}\right)\right]r_s^2$$

Theorem 1 below, which exploits the results of Lemma 5, computes the planar sensor density that is necessary to ensure k-coverage of a planar field of interest (solution to sub-problem 2 in 1.1). It is based on the sensor deployment within the inner diamond area of our generalized irregular hexagon $IrHx(r_s/n)$.

Theorem 1. *(Planar Sensor Density): The planar sensor density $\lambda(k, r_s, n)$, which is required to k-cover a planar field of interest, is computed as follows:*
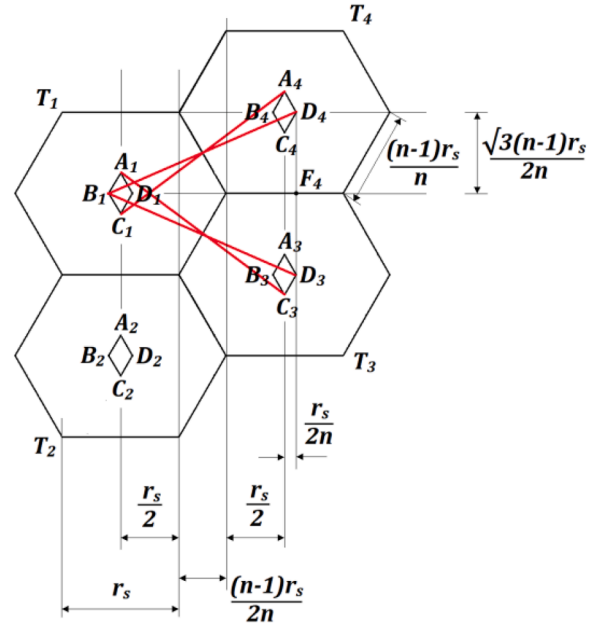

Fig. 6. Inner diamond areas of adjacent generic irregular hexagons $IrHx(r_s/n)$.

$$\lambda(k, r_s, n) = \frac{k}{\left[\pi + \frac{(3n^2-6n+2)\sqrt{3}}{4n^2} - \frac{\sqrt{4n^2-1}}{n^2} - 4\sin^{-1}\left(\frac{1}{2n}\right)\right]r_s^2}$$

where r_s is the radius of the sensing range of the sensors, and k and n are natural numbers, such that $k \geq 1$ and $n > 1$.

Proof: The planar sensor density of an irregular hexagonal tile is the number of sensors deployed per unit area of the tile. Hence, given that k sensors need to be placed within the inner diamond area to k-cover an area whose size is A_k, this planar sensor density, denoted by $\lambda(k, r_s, n)$, is given by:

$$\lambda(k, r_s, n) = \frac{k}{A_k}$$

By substituting the value of A_k from Lemma 5, we get:

$$\lambda(k, r_s, n) = \frac{k}{\left[\pi + \frac{(3n^2-6n+2)\sqrt{3}}{4n^2} - \frac{\sqrt{4n^2-1}}{n^2} - 4\sin^{-1}\left(\frac{1}{2n}\right)\right]r_s^2}$$

Notice that the planar sensor density $\lambda(k, r_s, n)$ depends only on the coverage degree k, the radius r_s of the sensing range of sensors, and the natural number $n > 1$.

Remark 1. It is evident that our result from Theorem 1 is a lesser planar sensor density compared to that of the one deduced in Reuleaux triangle-based approaches [7–10,14], square-based approach [31] and regular hexagon-based approach [11], regardless of the value of n. This indicates that the total k-coverage area as well as the total tile area is higher for our Irregular hexagonal approach compared to Reuleaux triangle-based approaches [7–10,14], square-based approach [31] and regular hexagon-based approach [11], and that our approach achieves k-coverage of a planar field of interest with a smaller number of sensors compared to existing tessellation-based research [7–11,14,31].

Lemma 6 indicates the required relationship that should exist between the radii of the sensing and communication ranges of sensors for maintaining network connectivity of PWSNs (solution to sub-problem 3 in 1.1). This relationship is the key attribute for attaining connected k-coverage during the entire operational lifetime of PWSNs using our

generalized irregular hexagon, $IrHx(r_s/n)$.

Lemma 6. *(Network Connectivity): Given an irregular hexagonal tessellation-based k-coverage configuration, all the sensors are mutually connected to each other, directly or indirectly, if the radii of their sensing and communication ranges, r_s and r_c respectively, comply with the following inequality:*

$$r_c \geq \frac{\sqrt{3n^2 + 1}}{n} r_s$$

Proof: The essential condition for maintaining network connectivity is that two farthest sensors should be able to communicate with each other. Let us consider the adjacent generic irregular hexagonal configuration comprising the tiles T_1, T_2, T_3 and T_4, as shown in Fig. 6. Also, sensors are far from each other when they are placed at the vertices of inner diamond areas that correspond to adjacent irregular hexagonal tiles. For inner diamond $A_1B_1C_1D_1$ of tile T_1, if a sensor s_i is placed at vertex B_1, the farthest sensor s_j from s_i should be placed at either vertex D_3 of inner diamond $A_3B_3C_3D_3$ of tile T_3, or vertex D_4 of inner diamond $A_4B_4C_4D_4$ of tile T_4. We also have two other sensor placements, vertex A_1 to vertex C_3 and vertex C_1 to vertex A_4, that are equivalent to the ones discussed above, but as all the lengths are equal, we will compute the length of $\overline{B_1D_4}$. The length of $\overline{B_1D_4}$ is computed as follows:

$$\overline{B_1D_4}^2 = \overline{B_1F_4}^2 + \overline{F_4D_4}^2 = \left(\frac{r_s}{2n} + \frac{r_s}{2} + \frac{(n-1)r_s}{2n} + \frac{r_s}{2} + \frac{r_s}{2n}\right)^2 + \left(\frac{\sqrt{3}(n-1)r_s}{2n}\right)^2 = \left[\frac{(3n^2+1)r_s^2}{n^2}\right]$$

$$\Rightarrow \overline{B_1D_4} = \frac{\sqrt{3n^2+1}}{n} r_s$$

Therefore, $r_c \geq \frac{\sqrt{3n^2+1}}{n} r_s$. ∎

Remark 2. It is easy to prove the following inequality for our generalized irregular hexagon, $IrHx(r_s/n)$, holds for any value of n:

$$\frac{\sqrt{3n^2+1}}{n} < 2$$

where n is a natural number and $n > 1$.

Let us consider the domain of n, i.e., $n > 1$. Then, we get, $n^2 > 1 \Rightarrow n^2 + 3n^2 > 1 + 3n^2 \Rightarrow 4n^2 > 1 + 3n^2 \Rightarrow 2n > \sqrt{1 + 3n^2} \Rightarrow 2 > \frac{\sqrt{3n^2+1}}{n}$. Therefore, $\frac{\sqrt{3n^2+1}}{n} < 2$.

Based on the result of Lemma 6, it is evident that our approach necessitates $r_c \geq \frac{\sqrt{3n^2+1}}{n} r_s < 2r_s$, which is better compared to the result found by Wang et al. [5,6], which requires $r_c \geq 2r_s$. This indicates that our approach can work well with lower communication range sensors and requires lesser powered sensors than those of Wang et al. [5,6].

Leveraging all the above-examined and established mathematical properties, we introduce our connected k-coverage protocol, called k-InDi, which utilizes the inner diamond areas of the irregular hexagonal tiles of the tessellation of a planar field of interest.

5. K-Coverage protocol using inner diamonds

In this section, we discuss our proposed *k*-coverage protocol using *In*ner *Di*amonds (*k*-InDi), which is a centralized protocol based on a deterministic sensing model. Our protocol *k*-InDi has two major phases:

- Phase 1: Irregular Hexagonal tessellation generation
- Phase 2: Sensor selection and scheduling

where Phase 1 generates irregular hexagonal tessellation with inner diamond areas for each tile, ensuring that *k*-coverage of each tile is achieved and all sensors located in the inner diamond area of each tile can communicate with sensors located in the inner diamond areas of the neighboring tiles, and Phase 2 is responsible for selection and scheduling of sensors (solution to sub-problem 4 in 1.1) for minimizing energy/power consumption of sensors during *k*-coverage process, thus maximizing the operational network lifetime. Next, we discuss both phases in detail.

5.1. Tessellation generation

In this first phase, before initiating the *k*-coverage rounds, the sink tessellates a planar field of interest using regular hexagonal tiles of side length r_s/n, based on the value of n. Then, as discussed earlier, it initially generates one base irregular hexagon, $IrHx(r_s/n)$, using a diamond area. Moreover, using this base hexagon, the sink tessellates over the existing regular hexagonal tessellation. This newly generated tessellation using our generalized irregular hexagon, $IrHx(r_s/n)$, remains static (or unchanged) throughout the *k*-coverage process. Also, the inner diamond areas of each irregular hexagonal tile act as the bounded area for the sensor selection process for *k*-covering the entire planar field of interest.

5.2. Sensor selection and scheduling

The sink chooses the sensors and arranges for participation in the *k*-coverage rounds during this second phase. The main objective of this phase is to select and duty-cycle (or schedule) the sensors in a way that maintains a nearly constant energy depletion rate over the course of the whole *k*-coverage rounds. This implies that all the sensors have comparable lifetimes. The secondary objective of this phase is to reduce battery-power consumption in every *k*-coverage round, which implicitly ensures prolonged lifetime of the individual sensors, thus, extending the operational lifetime of the network. Every sensor is assigned a unique identifier (*id*) by the sink, and the selection process for sensor scheduling (or duty-cycling) for each *k*-coverage round takes into account the sensors' locations and remaining battery power.

Initially, all the sensors are in sleep mode. In addition, at the beginning of each *k*-coverage round, the sleep-mode sensors awaken in order to receive the scheduling instructions from the sink. The scheduled sensors may occasionally be outside the interior diamond sections but not within. In these situations, the sensors would move outside the confines of the inner diamond area of their asymmetric hexagonal tile. This type of sensor mobility consumes battery power. The schedule, which contains a list of the scheduled sensors' *ids* for that particular *k*-coverage round, is broadcast at the end of this step by the sink to all the sensors. A sensor checks to see whether its *id* is listed in the scheduling list after receiving the schedule. If this is the case, the sensor removes its *id* from the scheduling list, sends the modified schedule to its one-hop neighbors, and continues to be active for the *k*-coverage procedure. If not, it merely enters sleep mode after forwarding the schedule to its one-hop neighbors without making any changes to the scheduling list.

6. Lifetime estimation of our protocol

In this section, we will be evaluating the energy consumption of sensor per k-coverage round and the lifetime of overall PWSN based on our protocol k-InDi, discussed in previous section. Next we discuss the estimation of energy consumption of individual sensor and lifetime of PWSN in detail.

6.1. Energy consumption of sensor

In order to compute the energy consumption of individual sensor, we have to estimate the probabilities P_k that determines if a sensor participates in k-coverage process or not and P_{move} that determines if a sensor moves during k-coverage process or not.

Lemma 7 below determines the probability of a sensor being selected for the k-coverage process.

Lemma 7. *(k-Coverage Selection Probability): The probability that a sensor s is selected from N sensors of PWSN for active participation in k-coverage round is given by,*

$$P_k = \frac{kA_{FoI}}{NA_{Tile}}$$

where k is the degree of coverage, N is the total number sensors deployed in planar field of interest, A_{FoI} is the area of planar field of interest and A_{Tile} is the area of tile.

Proof: The probability P_k is the ratio of total number of sensors N_k actively participate per k-coverage round and the total number of sensors N deployed in the planar field of interest. Thus, we can write the probability P_k as

$$P_k = \frac{N_k}{N} = \frac{k \times n_{tiles}}{N}$$

and number of tiles n_{tiles} of a tessellation can be estimated as,

$$n_{tiles} = \frac{A_{FoI}}{A_{Tile}}$$

Therefore, probability of a sensor to be selected for k-coverage process P_k is,

$$P_k = \frac{kA_{FoI}}{NA_{Tile}}$$

Lemma 8 below computes the probability of a sensor selected k-coverage process is instructed to move towards the inner diamond area of the tile.

Lemma 8. *(Movement Instruction Probability): The probability that a sensor s, which is selected for k-coverage process, is instructed to move towards/inside of inner diamond area of a tile by the sink, is given by,*

$$P_{move} = \frac{n(3n-4)}{(n-1)(3n-1)}$$

where n is slicing factor of our tessellation and $n > 1$.

Proof: The probability P_{move} is determined by computing the probability P'_{move}, that a sensor which is selected for k-coverage process is given no movement instructions by the sink. Moreover, the probability P'_{move} is the ratio of number of sensors N_{ID} present in the inner diamond of the tile to number of sensors N_{Tile} present in the entire tile. Thus, we can write P'_{move} as,

$$P'_{move} = \frac{N_{ID}}{N_{Tile}}$$

But, from Assumption 1, we have, $N_{ID} = \rho \times A_{ID}$ and $N_{Tile} = \rho \times A_{Tile}$, where A_{ID} is the area of inner diamond of tile and A_{Tile} is the area of irregular hexagonal tile. Thus, we have P'_{move} as,

$$P'_{move} = \frac{\rho \times A_{ID}}{\rho \times A_{Tile}} = \frac{1}{(n-1)(3n-1)}$$

Therefore,

$$P_{move} = 1 - P'_{move} = 1 - \frac{1}{(n-1)(3n-1)} = \frac{n(3n-4)}{(n-1)(3n-1)}$$

Leveraging the results of Lemma 7 and Lemma 8, Theorem 2 computes the total energy consumption of a sensor based on our protocol k-InDi.

Theorem 2. *(Sensor's Energy Consumption): The total energy (or) battery power consumed by a sensor s per each k-coverage round is given by,*

$$E_{consume} = \frac{kA_{FoI}}{NA_{Tile}}\left(E_t(d) + E_r + \frac{n(3n-4)d_{move}E_{move}}{(n-1)(3n-1)}\right) + E_{sleep}\left(1 - \frac{kA_{FoI}}{NA_{Tile}}\right)$$
$$+ E_{idle}$$

where k is degree of coverage, N is total number of sensors deployed in planar field of interest, A_{FoI} is the area of planar field of interest, A_{Tile} is the area of tile, $E_t(d)$ is the energy consumed for data transmission, E_r is the energy consumed for data reception, E_{sleep} is the energy consumed during sleep mode, E_{idle} is the energy consumed during awake mode, E_{move} is the energy consumed for movement per distance moved, d_{move} is the distance moved by sensor and n is the slicing factor of the tessellation ($n > 1$).

Proof: Based on the sensor scheduling phase of our protocol k-InDi, a sensor participating in k-coverage round utilizes energy for data transmission, data reception and movement (only if instructed by sink to move to specific location) and a sensor that is not participating in k-coverage round utilizes energy to stay in sleep mode. Moreover, every sensor at the start of each k-coverage round stays in awake mode for receiving and processing the instructions. Therefore, we can estimate the energy consumption of a sensor in PWSN utilizing our approach as,

$$E_{consume} = P_k(E_t(d) + E_r + P_{move}d_{move}E_{move}) + E_{sleep}(1 - P_k) + E_{idle}$$

By substituting the values of the probabilities P_k (Lemma 7) and P_{move} (Lemma 8) in the above equation, we get,

$$E_{consume} = \frac{kA_{FoI}}{NA_{Tile}}\left(E_t(d) + E_r + \frac{n(3n-4)d_{move}E_{move}}{(n-1)(3n-1)}\right) + E_{sleep}\left(1 - \frac{kA_{FoI}}{NA_{Tile}}\right)$$
$$+ E_{idle}$$

It is evident from Theorem 2 that energy consumption of a sensor in PWSN, based on tessellation based approach, is inversely proportional to the area of the tile, which is used for tessellating the planar field of interest.

Remark 3. From Remark 1, the area of tile is larger for our Irregular hexagon approach compared to Reuleaux triangle-based approaches [7–10,14], square-based approach [31] and regular hexagon-based approach [11]. This indicates that our approach achieves lower energy consumption of sensor compared to existing tessellation-based research [7–11,14,31], therefore making our approach more energy-efficient.

6.2. Lifetime of PWSN

Theorem 3 below computes the lifetime of PWSN, leveraging the results of Theorem 2.

Table 4a

$\lambda(k, r_s, n)$ as a function of n.

n	2	3	4	5
$\lambda(k, r_s, n)$	$\dfrac{0.7251\,k}{r_s^2}$	$\dfrac{0.4267\,k}{r_s^2}$	$\dfrac{0.3511\,k}{r_s^2}$	$\dfrac{0.3168\,k}{r_s^2}$

Table 4b

$\lambda(k, r_s, n)$ as a function of n (cont'd).

n	10	20	100	∞
$\lambda(k, r_s, n)$	$\dfrac{0.2639\,k}{r_s^2}$	$\dfrac{0.2431\,k}{r_s^2}$	$\dfrac{0.2252\,k}{r_s^2}$	$\dfrac{0.2252\,k}{r_s^2}$

Theorem 3. *(Operational Network Lifetime): The lifetime of PWSN that ensures k-coverage of a planar field of interest, can be estimated as,*

$$\mathscr{L} = \frac{E_{init}N^2 A_{Tile}^2}{kA_{FoI}\left[kA_{FoI}\left(E_t(d) + E_r + \frac{n(3n-4)d_{move}E_{move}}{(n-1)(3n-1)}\right) + E_{sleep}(NA_{Tile} - kA_{FoI}) + NA_{Tile}E_{idle}\right]}$$

where k is degree of coverage, N is total number of sensors deployed in planar field of interest, A_{FoI} is the area of planar field of interest, A_{Tile} is the area of tile, $E_t(d)$ is the energy consumed for data transmission, E_r is the energy consumed for data reception, E_{init} is the initial energy (or) battery power of sensor, E_{sleep} is the energy consumed during sleep mode, E_{idle} is the energy consumed during awake mode, E_{move} is the energy consumed for movement per distance moved, d_{move} is the distance moved by sensor and n is the slicing factor of the tessellation ($n > 1$).

Proof: Let us consider the equation of lifetime of PWSN $\mathscr{L}$ from Section 3.4, where E_{init}^N is total initial energy (or) battery power of the entire PWSN and $E_{consume}^k$ is total energy (or) battery power consumption of all active sensors participating in k-coverage process,

$$\mathscr{L} = \frac{E_{init}^N}{E_{consume}^k}$$

The value of E_{init}^N is,

$$E_{init}^N = N \times E_{init}$$

and the value of $E_{consume}^k$ is,

$$E_{consume}^k = k \times n_{tiles} \times E_{consume} = \frac{kA_{FoI}E_{consume}}{A_{Tile}}$$

Now by considering the value of $E_{consume}$ from Theorem 2, we get,

$$\mathscr{L} = \frac{NE_{init}A_{Tile}}{kA_{FoI}E_{consume}} = \frac{E_{init}N^2 A_{Tile}^2}{kA_{FoI}\left[kA_{FoI}\left(E_t(d) + E_r + \frac{n(3n-4)d_{move}E_{move}}{(n-1)(3n-1)}\right) + E_{sleep}(NA_{Tile} - kA_{FoI}) + NA_{Tile}E_{idle}\right]}$$

It is evident from Theorem 3 that the lifetime of the PWSN, based on our tessellation-based approach, is also directly proportional to the area of the tile, which is used for tessellating the planar field of interest.

Remark 4. From Remark 1, the area of tile is larger for our Irregular

hexagon approach compared to Reuleaux triangle-based approaches [7–10,14], square-based approach [31] and regular hexagon-based approach [11]. This indicates that the operational network lifetime of our protocol k-InDi will be higher than that of protocols developed in [7–11,14,31], which are proved to be better than CCP [5,6], a well-known protocol.

7. Performance evaluation

In this section, we present the performance of our proposed connected k-coverage protocol, k-InDi, and compare our results with an existing WSN protocol. We have used an open-source high-level WSN simulator [33] by darolt, developed in *Python* and *C++* programming languages. Moreover, we updated the network component of the simulator to model the tessellation-based k-coverage theories by accepting the tiling shape and degree of coverage k as inputs. Apart from the simulator's existing energy plot functionality, additionally we added plot functionalities for the experiments discussed in the subsequent sections. First, we briefly describe our simulation environment and its parameters, and then discuss the simulation results of our proposed protocol for solving the connected k-coverage problem in PWSNs Table 4a,4b.

7.1. Simulation environment

No matter the type of polygonal shape, such as a triangle, square, trapezium, hexagon, or decagon, to mention a few, our connected k-coverage protocol, k-InDi, can be applied to any planar field of interest. In these experiments, we consider a square-shaped planar field. As previously mentioned in our energy model (Section 3.3), all types of battery power consumption, including data sensing, data transmission, data reception, sensor mobility, and control messages, are taken into account to ensure that our connected k-coverage protocol, k-InDi, operates as intended. We used the IEEE 802.11 distributed coordinated function with CSMA/CA as the underlying MAC protocol. Furthermore, we consider a radio interference model given the pervasiveness of other 2.4 GHz radio sources. All simulations are performed on a 10th Gen Intel (R) Core(TM) i7–10750H 2.60 GHz CPU with 16 GB of RAM, under the environment of a 64-bit Windows 11 operating system, and network parameters used for simulations are listed in Table 5.

7.2. Simulation results

In this section, we demonstrate the simulation results for our k-InDi protocol. In Section 7.3, we contrast RCH$_k$ [11] and k-InDi.

Fig. 8 shows the variation of theoretical planar sensor density λ_{theo} (based on Theorem 1) and simulation-based planar sensor density λ_{sim} (for our k-InDi protocol) with changing sensing radius r_s, degree of coverage k, and factor n. Fig. 8(a) plots λ_{theo} and λ_{sim} while varying r_s,

Table 5
Simulation parameters of the network.

Parameter Name	Description	Value
S	Side length of the Field of Interest	250 m
N	Total number of sensors deployed	1000
E_{init}	Initial battery power	70 J
E_e	Electronical energy consumption	50 nJ/bit
ε_{fs}	Transmitter amplifier in free space	10 pJ/bit/m^2
ε_{mp}	Transmitter amplifier in multi-path	0.0013 pJ/bit/m^4
E_{move}	Energy consumption for displacing a sensor	[0.008 – 0.012] J/m
E_{idle}	Energy consumption for idle mode of a sensor	0.012 J
E_{sleep}	Energy consumption for sleep mode of a sensor	0.0003 J
r_s	Sensing range of sensor	25 m
r_c	Communication range of sensor	50 m
k	Degree of Coverage	3
n	Slicing factor	5

where $k = 3$ and $n = 5$. As expected, both λ_{theo} and λ_{sim} decrease with increasing r_s for constant values of k and n. Fig. 8(b) plots λ_{theo} and λ_{sim} while varying k, where $r_s = 25$ m and $n = 5$. As expected, we observe that both λ_{theo} and λ_{sim} increase with increasing k for constant values of r_s and n. Fig. 8(c) plots λ_{theo} and λ_{sim} while varying n, where $k = 3$ and $r_s = 25$ m. Likewise and as expected, both λ_{theo} and λ_{sim} decrease with increasing n for constant values of k and r_s. Though the behavior is as expected, there is a slight difference between the λ_{theo} and λ_{sim} that is clearly visible, and our protocol k-InDi requires slightly higher sensor density compared to that computed in Theorem 1. This is because, as calculated in Theorem 1, λ_{theo} considers all the common k-cover regions around the sides of the irregular hexagonal tile, which includes the hexagonal area as well as the six curved areas on each side of each irregular hexagon tile. These curved areas form over-k-covered regions in the planar field of interest that are not considered in λ_{sim}.

Fig. 9 shows the required number of active sensors n_a compared to that of the number of deployed sensors n_d for our k-InDi protocol. In Fig. 9(a), we performed experiments by varying r_s; in Fig. 9(b), we performed experiments by varying k; and in Fig. 9(c), we performed experiments by varying n. It is evident that for higher values of r_s and n, we require lesser number of sensors, whereas for higher values of k we require higher number of sensors for providing the desired degree of coverage k. Moreover, from all experiments, it is clear that n_a only depends on the values of r_s, n and k, but not n_d.

Fig. 10 plots the variation of degree of coverage k with regard to the number of active sensors n_a for our k-InDi protocol. The experiments in Fig. 10(a) are conducted by varying r_s for a constant value of $n = 5$, whereas in Fig. 10(b), experiments are conducted by varying n for a constant value of $r_s = 25$ m. It is clear that k increases proportionally with n_a, where it is visible that for a constant number of active sensors, k increases with increase in r_s, which indicates that a larger planar field of interest can be k-covered. In addition, it is evident that k increases with increase in n, which indicates that a smaller number of larger irregular hexagonal tiles can be used for the k-coverage process Fig. 7.

7.3. Comparison of k-InDi with RCH_k

In this section, we compare k-InDi with RCH$_k$ [11]. As discussed earlier in Section 2, Ammari's work [11] examined the issue of k-coverage in PWSNs and suggested a regular hexagon-based k-coverage protocols, while considering a degree of coverage $k \geq 3$. Hence, we baseline the degree of coverage $k = 3$ for comparing our protocol k-InDi with Ammari's RCH$_k$ protocol [11], which is proved to be better than CCP [5,6] which is a well-known protocol.

Fig. 11 plots the comparison of the simulation results that are obtained for the planar sensor density λ of both k-InDi and RCH$_k$ protocols with varying sensing radius r_s in Fig. 11(a), varying degree of coverage k in Fig. 11(b), and varying factor n in Fig. 11(c). From the plots in Fig. 11 (a) and (b), it is clear that our protocol k-InDi has lower sensor density λ compared to that of RCH$_k$ [11]. Therefore, it is evident that for a specific coverage degree k, our protocol k-InDi achieves k-coverage of the planar field with lesser number of sensors compared to that of RCH$_k$. In other words, we can say that for specific fixed value of sensor density λ, our protocol k-InDi offers higher degree of coverage k compared to RCH$_k$. Also, for a constant value of sensor density λ, k-InDi requires low-sensing-range sensors for achieving the desired coverage degree k. Thus, it is clear that our proposed k-coverage protocol k-InDi requires less-powered sensors to k-cover a planar field compared to RCH$_k$ [11]. Furthermore, from Fig. 11(c), we observe that with increase in the factor n, the value of the sensor density λ decreases proportionally, for constant values of the radius r_s of the sensing range of the sensors and the degree of coverage k. This indicates that our protocol achieves same degree of coverage for different λ. Also, it is clear that for higher value of n, our protocol achieves the desired degree of coverage with lesser number of homogeneous sensors (i.e., sensors having the same characteristics, including their initial battery power, sensing range, and communication range).
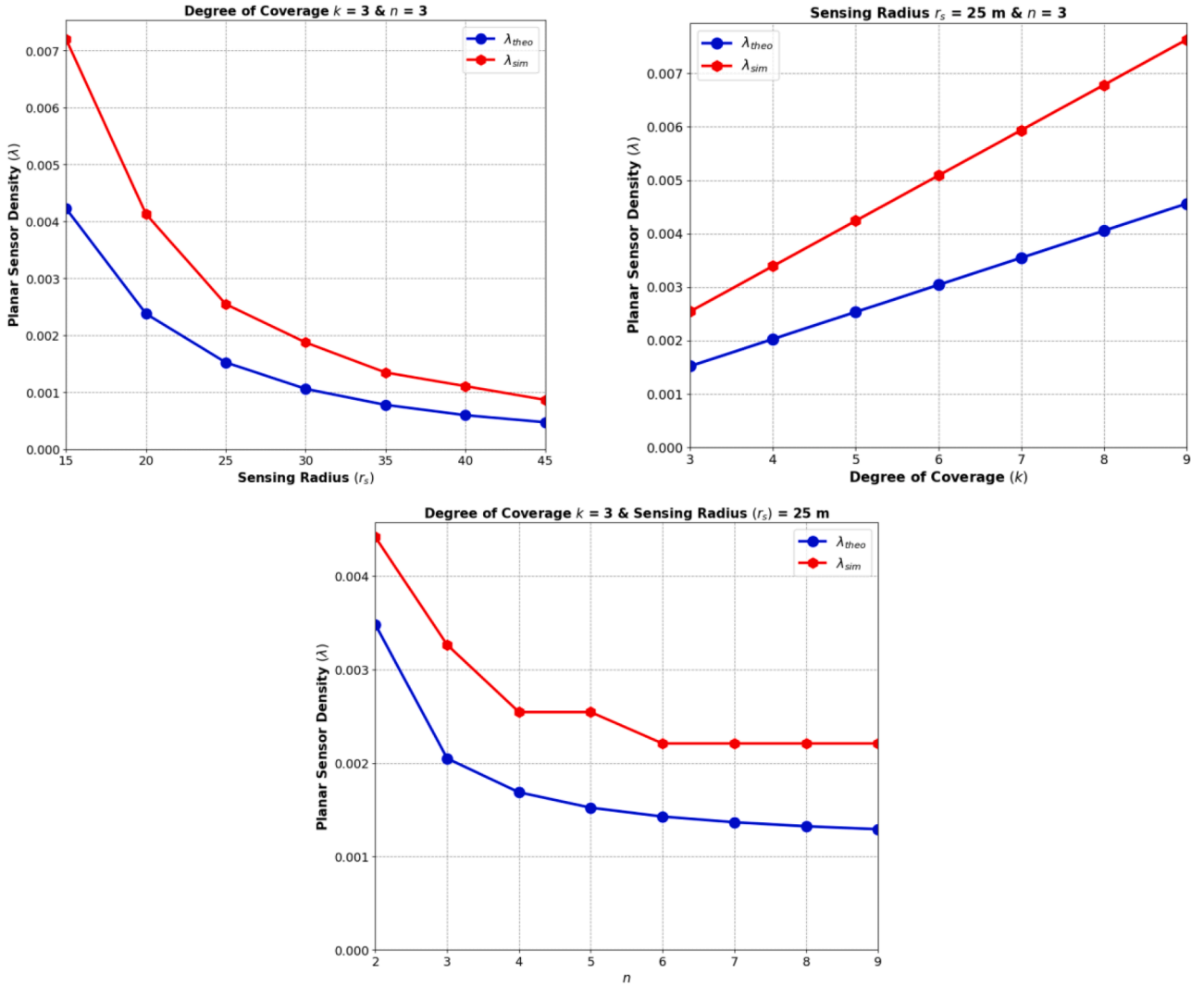
1. *IrHx_Tiles* = Tessellate_Field_of_Interest() /* *Generate IrHx(r_s/n) tessellation and returns list of tiles* */
2. *kCov_Sensors* = {} /* *Empty set* */
3. **For** *Tile* **in** *IrHx_Tiles* **Do**
    Begin
    3.1. Select subset *S_{Tile}* of sensors located on the *Tile*.
    3.2. *j* = 1
    3.3. While *j* ≤ *k* **Do**   /* *k is expected coverage degree* */
        Begin
        3.4.1. Select one sensor *s* from *S_{Tile}*, with highest remaining energy.
        3.4.2. If *Location(s)* is outside of *Inner_Diamond(Tile)* **Then**
            3.4.2.1. *Add_Movement_Instructions(s)*
        3.4.3. *j* = *j* + 1
        3.4.4. Add sensor *s* to *kCov_Sensors* set.
        End
    End
4. **Return** *kCov_Sensors*
End

Fig. 7. Pseudo code for *k*-InDi protocol.

Fig. 8. Planar sensor density λ versus (a) sensing radius r_s, (b) degree of coverage k, and (c) factor n.

Fig. 12(a) shows the difference between k-InDi and RCH$_k$ k-coverage protocols in terms of the required total number of active sensors n_a compared to the total number of deployed sensors n_d. As inferred earlier from the results of Figs. 11, 12(a) proves that our k-InDi protocol achieves the same degree of coverage k with fewer active sensors. Fig. 12(b) plots degree of coverage k versus number of active sensors n_a for both k-InDi and RCH$_k$ protocols. It is clear that it supports our prior conclusion that for a given number of active sensors, k-InDi provides a higher coverage degree than RCH$_k$ [11]. As a result, given a particular targeted coverage degree k, our protocol k-InDi produces significant energy savings, hence increasing the operational lifetime of the underlying sensor network. This is because RCH$_k$ requires more active sensors, thus, incurring more energy for sensing and messaging among active sensors. That is, RCH$_k$ causes a communication overhead that prevents active sensors from cooperating with one another and providing the anticipated degree of coverage. As a result, RCH$_k$ network operations use more energy to k-cover the planar field of interest.

Fig. 13 plots the remaining energy versus time. It shows k-InDi and RCH$_k$ protocols' energy consumption rate and operational network lifetime. The results of this plot demonstrate our prior hypotheses that are deduced from the results of Fig. 12(a) and (b). It is clear that the operational network lifetime of k-InDi is greater than that of RCH$_k$, as estimated in Theorem 3.

Fig. 14(a) plots n_a versus r_s with $n = 5$, whereas Fig. 14(b) plots n_a versus r_c with $r_s = 25$ m and $n = 5$, for different values of k. In both cases,

we consider various values of k, with $k = 2$, 3 and 4. These results solidify our prior results that k-InDi offers higher coverage degree k with fewer active sensors compared to RCH$_k$. Also, k-InDi offers 4-coverage with n_a which is almost near to that required for 3-coverage by RCH$_k$. It is worth noting that n_a depends only on r_s, n, and k, and does not depend on the value of r_c. This is true for both k-InDi and RCH$_k$.

8. Conclusion

In this paper, we investigate the connected k-coverage problem in PWSNs using an irregular hexagonal tessellation-based approach. In particular, we address the sensor deployment problem by utilizing diamond areas in the tessellation and calculate the planar sensor density that is required to maintain k-coverage of a planar field of interest. Also, we establish a relationship for maintaining the network connectivity of all active sensors participating in k-coverage process, thus, ensuring connected k-coverage configurations during the network operation, with no coverage voids and connectivity holes. Furthermore, we propose a centralized k-coverage protocol, k-InDi, which attains the same desired degree of coverage ensured by RCH$_k$ [11] with fewer sensors. Also, we observe a significant reduction in the energy consumption rate and an increase in the network lifetime for k-InDi protocol compared to RCH$_k$ [11].

Our future work is five-fold. Firstly, we are interested in finding an optimum value of n, the proportionality factor used to standardize the
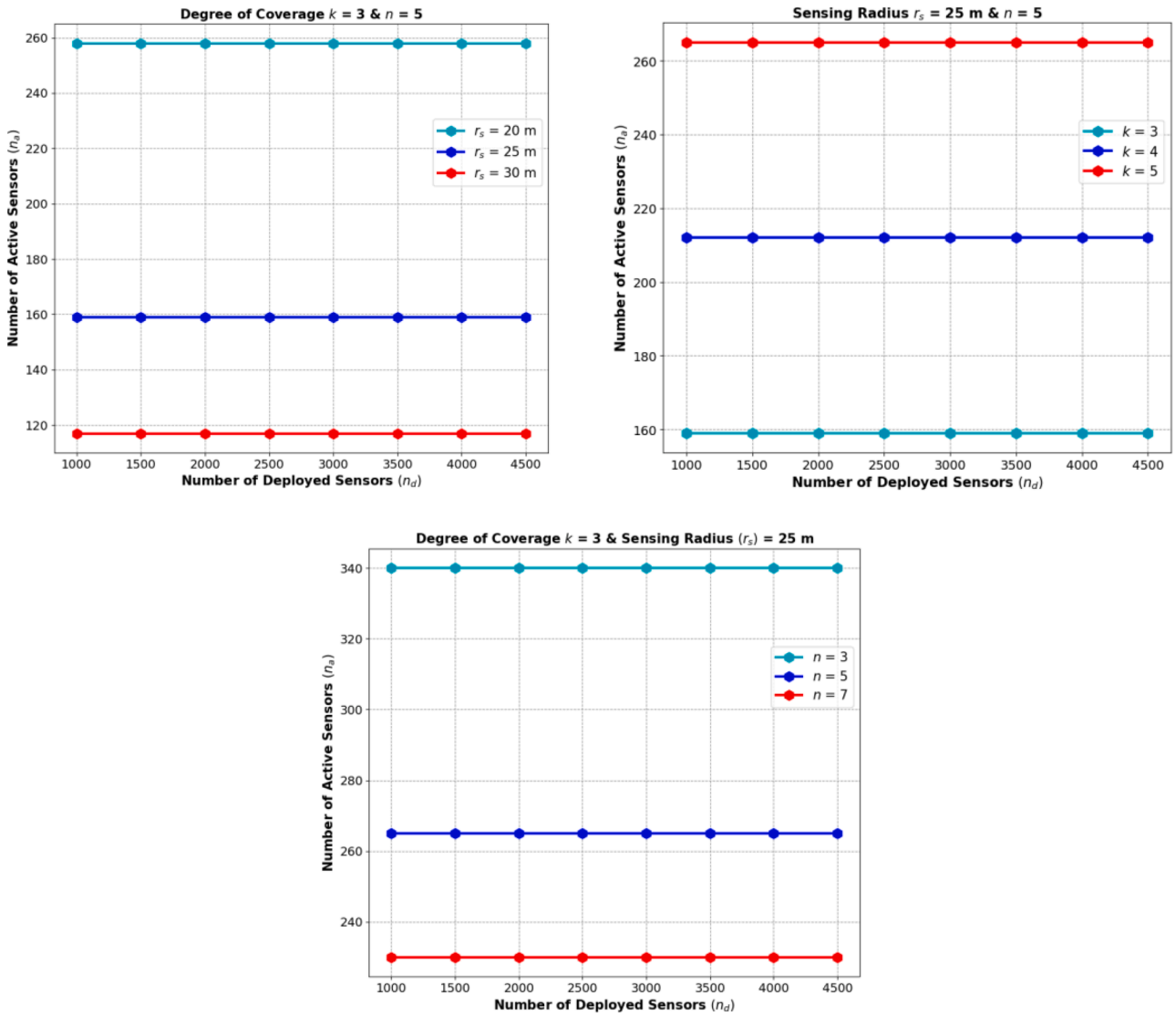
Fig. 9. Number of active sensors n_a versus number of deployed sensors n_d for different (a) sensing radius r_s, (b) degree of coverage k and (c) factor n.
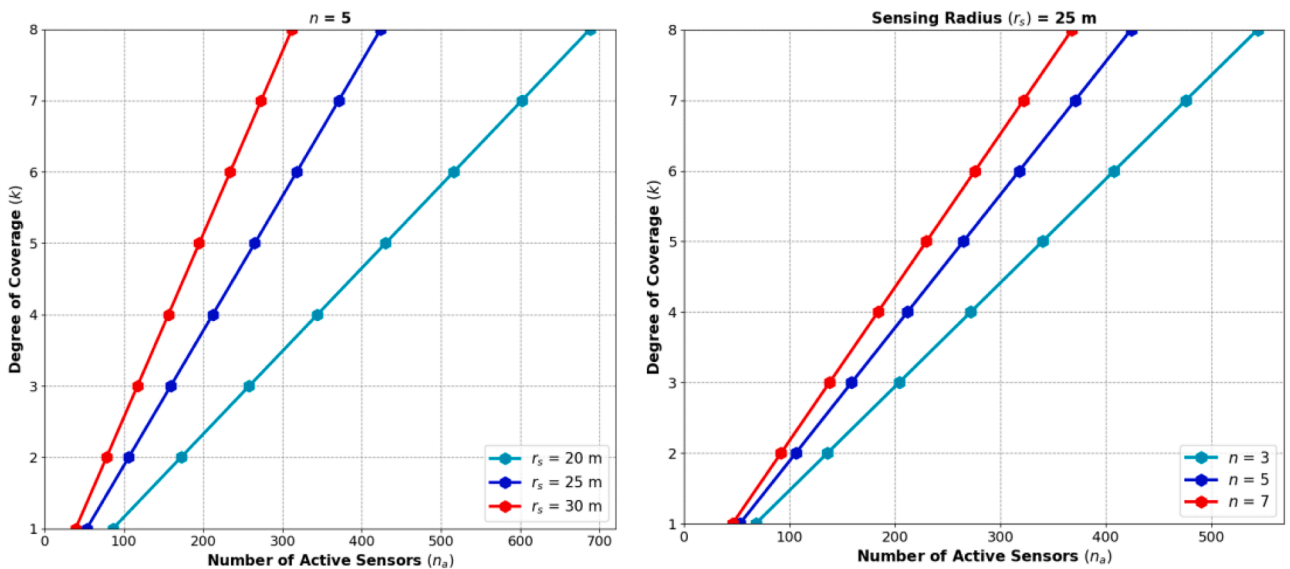

Fig. 10. Degree of coverage k versus number of active sensor n_a for different (a) sensing radius r_s and (b) factor n.
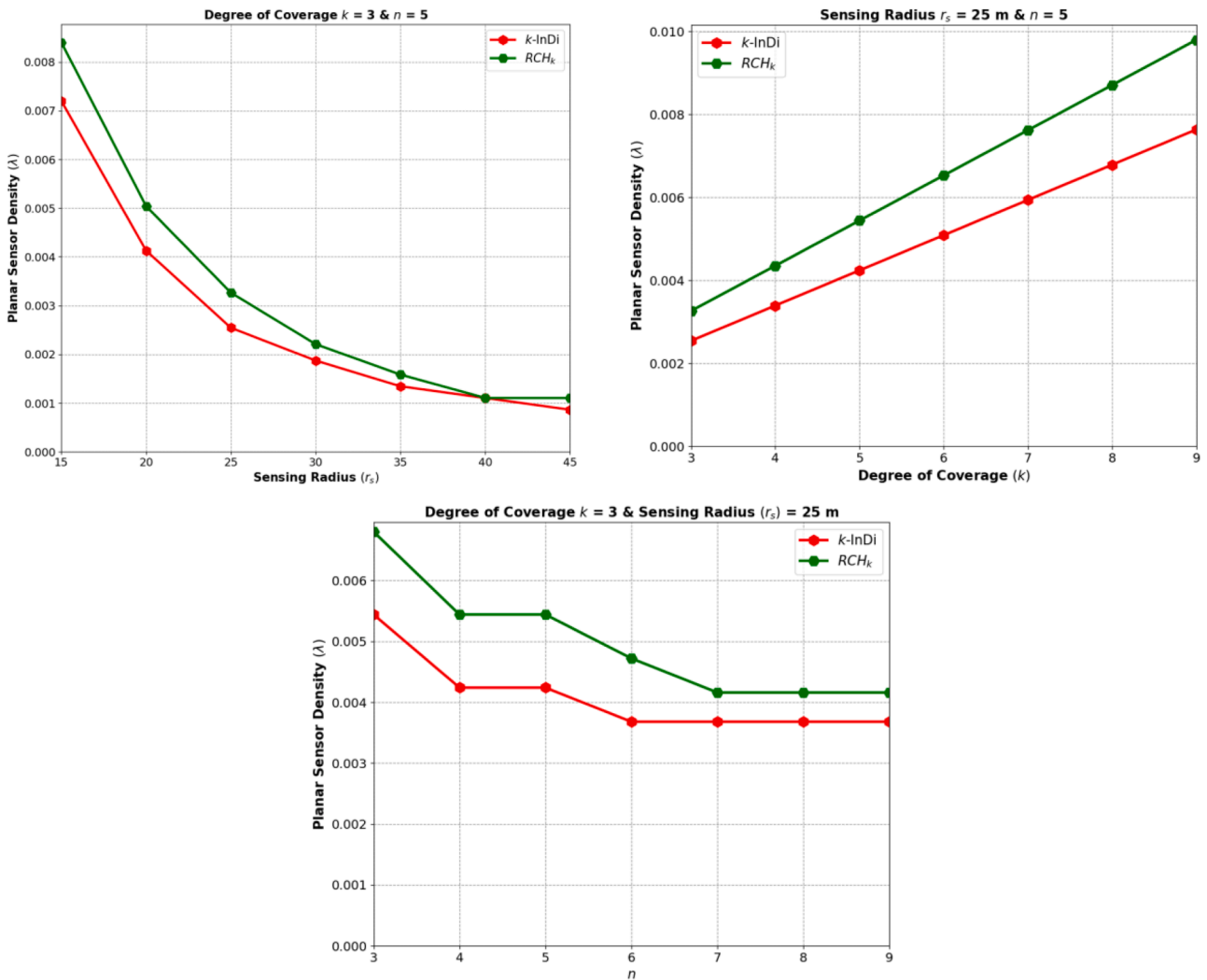
Fig. 11. Comparing k-InDi and RCH$_k$: Planar sensor density λ versus (a) sensing radius r_s, (b) degree of coverage k, and (c) factor n.
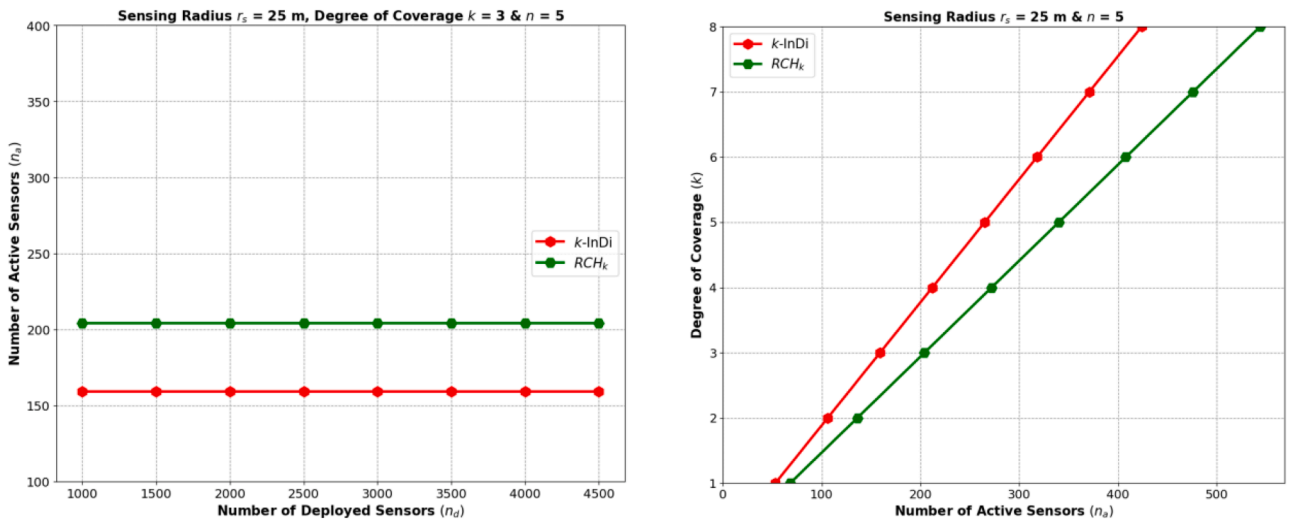

Fig. 12. Comparing k-InDi and RCH$_k$: (a) Number of active sensors n_a versus Number of deployed sensors n_d (b) Degree of coverage k versus Number of active sensor n_a.
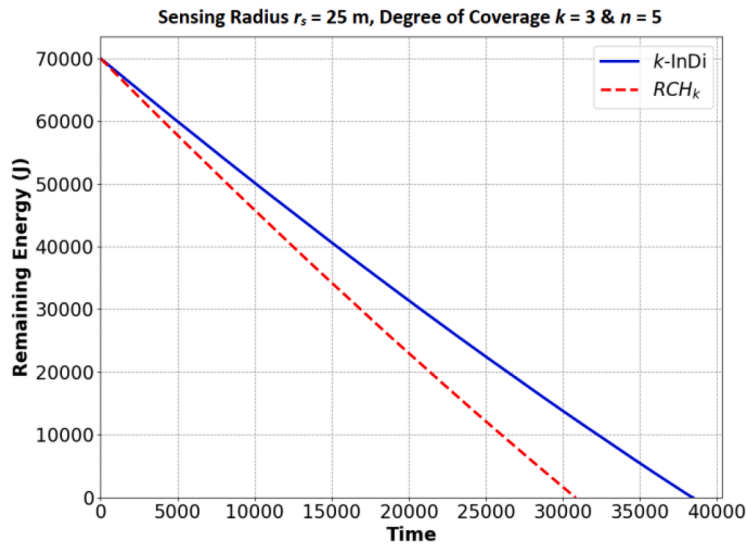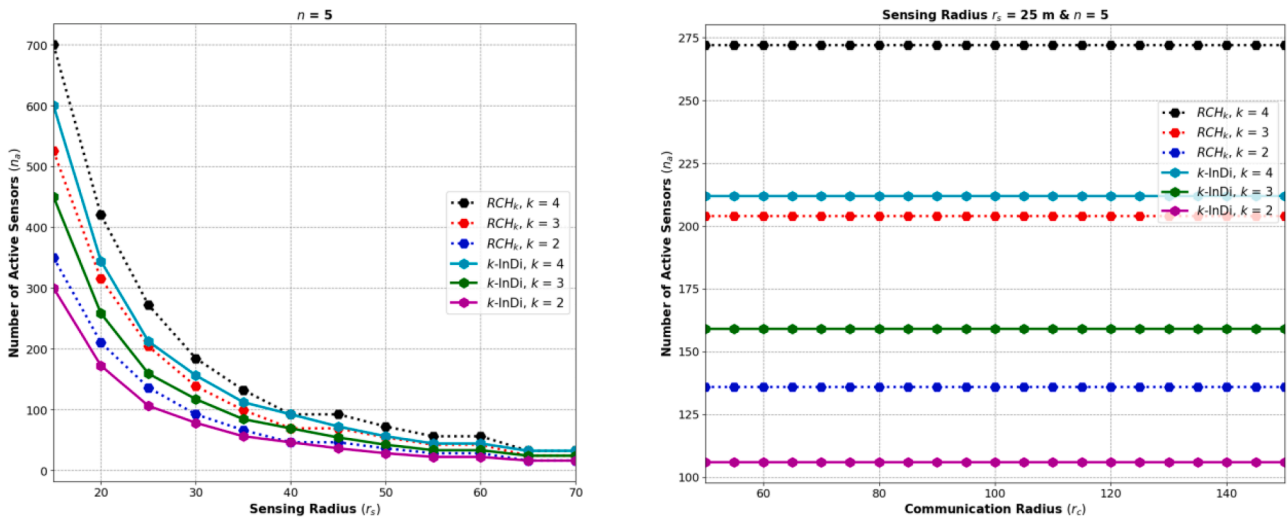
Fig. 13. Remaining energy versus time.

Fig. 14. Number of active sensors n_a versus (a) sensing radius r_s and (b) communication radius r_c.

regular hexagonal tessellation so as to generate the irregular hexagonal tessellation. Second, we intend to expand our research to account for heterogeneous sensors, which may not necessarily have the same initial energy, sensing range, and communication range [10,11]. Third, with a more comprehensive sensing model, which is stochastic [7,11] rather than deterministic, we concentrate on generalizing our work to take into account the irregularity of the sensing and communication ranges of the sensors. Fourth, we aim to expand the scope of our theory to further explore the issue of connected *k*-coverage in three-dimensional WSNs, such as underwater WSNs [29]. Finally, we plan to implement our proposed protocol using a sensor-testbed [30] in order to assess its feasibility and practicality in real-world scenarios.

Declaration of Competing Interest

The authors declare the following financial interests/personal relationships which may be considered as potential competing interests:

Habib M. Ammari reports financial support was provided by National Science Foundation. Habib M. Ammari reports a relationship with National Science Foundation that includes: funding grants.

Data availability

No data was used for the research described in the article.

References

[1] N. Bulusu, J. Heidemann, D. Estrin, GPS-less low-cost outdoor localization for very small devices, IEEE Pers. Commun. 7 (5) (2000) 28–34.

[2] W.B. Heinzelman, A.P. Chandrakasan, H. Balakrishnan, An application-specific protocol architecture for wireless microsensor networks, IEEE Trans. Wireless Commun. 1 (4) (2002) 660–670.

[3] F. Ye, G. Zhong, J. Cheng, S. Lu, L. Zhang, PEAS: a robust energy conserving protocol for long-lived sensor networks, in: Proceedings of the 23rd International Conference on Distributed Computing Systems, 2003. Proceedings, IEEE, 2003, pp. 28–37.

[4] Y.C. Wang, Y.C. Tseng, Distributed deployment schemes for mobile wireless sensor networks to ensure multilevel coverage, IEEE Trans. Parallel Distrib. Syst. 19 (9) (2008) 1280–1294.

[5] X. Wang, G. Xing, Y. Zhang, C. Lu, R. Pless, C. Gill, Integrated coverage and connectivity configuration in wireless sensor networks, in: Proceedings of the 1st

international conference on Embedded networked sensor systems, 2003, pp. 28–39.

[6] G. Xing, X. Wang, Y. Zhang, C. Lu, R. Pless, C. Gill, Integrated coverage and connectivity configuration for energy conservation in sensor networks, ACM Trans. Sens. Netw. (TOSN) 1 (1) (2005) 36–72.

[7] H.M. Ammari, Stochastic k-coverage in wireless sensor networks, in: Proceedings of the Wireless Algorithms, Systems, and Applications: 4th International Conference, Springer Berlin Heidelberg, 2009, pp. 125–134. WASA 2009, Boston, MA, USA, August 16-18, 2009. Proceedings 4.

[8] H.M. Ammari, S.K. Das, Centralized and clustered k-coverage protocols for wireless sensor networks, IEEE Trans. Comput. 61 (1) (2011) 118–133.

[9] H.M. Ammari, Investigating the energy sink-hole problem in connected $ k $-covered wireless sensor networks, IEEE Trans. Comput. 63 (11) (2013) 2729–2742.

[10] H.M. Ammari, A unified framework for k-coverage and data collection in heterogeneous wireless sensor networks, J. Parallel Distrib. Comput. 89 (2016) 37–49.

[11] H.M. Ammari, Connected k-coverage in two-dimensional wireless sensor networks using hexagonal slicing and area stretching, J. Parallel Distrib. Comput. 153 (2021) 89–109.

[12] J. Yu, S. Ren, S. Wan, D. Yu, G. Wang, A stochastic k-coverage scheduling algorithm in wireless sensor networks, Int. J. Distrib. Sens. Netw. 8 (11) (2012) 746501.

[13] C. Qiu, H. Shen, K. Chen, An energy-efficient and distributed cooperation mechanism for $ k $-coverage hole detection and healing in WSNs, IEEE Trans. Mob. Comput. 17 (6) (2017) 1247–1259.

[14] J. Yu, S. Wan, X. Cheng, D. Yu, Coverage contribution area based $ k $-coverage for wireless sensor networks, IEEE Trans. Veh. Technol. 66 (9) (2017) 8510–8523.

[15] Z. Sun, C. Li, X. Xing, H. Wang, B. Yan, X. Li, K-degree coverage algorithm based on optimization nodes deployment in wireless sensor networks, Int. J. Distrib. Sens. Netw. 13 (2) (2017), 1550147717693242.

[16] F. Abbasi, A. Mesbahi, J.M. Velni, A new voronoi-based blanket coverage control method for moving sensor networks, IEEE Trans. Control Syst. Technol. 27 (1) (2017) 409–417.

[17] M. Chenait, B. Zebbane, N. Badache, A new k-coverage model to determine redundant sensors in wireless sensor networks, in: Proceedings of the 2018 International Conference on Smart Communications in Network Technologies (SaCoNeT), IEEE, 2018, pp. 149–154.

[18] P. Hoyingcharoen, W. Teerapabkajorndet, Expected probabilistic detection and sink connectivity in wireless sensor networks, IEEE Sens J 19 (12) (2019) 4480–4493.

[19] M. Torshizi, M.J. Sheikhzadeh, Optimum K-coverage in wireless sensor network with no redundant node by cellular learning automata, Wirel. Pers. Commun. 110 (2) (2020) 545–562.

[20] N.N. Qin, J.L. Chen, An area coverage algorithm for wireless sensor networks based on differential evolution, Int. J. Distrib. Sens. Netw. 14 (8) (2018), 1550147718796734.

[21] M. Krishnan, V. Rajagopal, S. Rathinasamy, Performance evaluation of sensor deployment using optimization techniques and scheduling approach for K-coverage in WSNs, Wirel. Netw. 24 (2018) 683–693.

[22] M. Elhoseny, A. Tharwat, X. Yuan, A.E. Hassanien, Optimizing K-coverage of mobile WSNs, Expert Syst. Appl. 92 (2018) 142–153.

[23] C. Naik, D.P. Shetty, Differential evolution meta-heuristic scheme for k-coverage and m-connected optimal node placement in wireless sensor networks, Int. J. Comput. Inf. Syst. Ind. Manag. Appl 11 (2019) 132–141.

[24] S. Harizan, P. Kuila, Nature-inspired algorithms for k-coverage and m-connectivity problems in wireless sensor networks, Des. Framew. Wirel. Netw. (2020) 281–301.

[25] P. Natarajan, L. Parthiban, k-coverage m-connected node placement using shuffled frog leaping: nelder–Mead algorithm in WSN, J. Ambient Intell. Humaniz. Comput. (2020) 1–16.

[26] K. Tarnaris, I. Preka, D. Kandris, A. Alexandridis, Coverage and k-coverage optimization in wireless sensor networks using computational intelligence methods: a comparative study, Electronics 9 (4) (2020) 675 (Basel).

[27] A. Alibeiki, H. Motameni, H. Mohamadi, A new genetic-based approach for solving k-coverage problem in directional sensor networks, J. Parallel Distrib. Comput. 154 (2021) 16–26.

[28] S. Elloumi, O. Hudry, E. Marie, A. Martin, A. Plateau, S. Rovedakis, Optimization of wireless sensor networks deployment with coverage and connectivity constraints, Ann. Oper. Res. 298 (2021) 183–206.

[29] A. Boukerche, P. Sun, Design of algorithms and protocols for underwater acoustic wireless sensor networks, ACM Comput. Surv. (CSUR) 53 (6) (2020) 1–34.

[30] P. Appavoo, E.K. William, M.C. Chan, M. Mohammad, Indriya 2: a heterogeneous wireless sensor network (WSN) testbed, in: Proceedings of the Testbeds and Research Infrastructures for the Development of Networks and Communities: 13th EAI International Conference, Springer International Publishing, 2019, pp. 3–19. TridentCom 2018, Shanghai, China, December 1-3, 2018, Proceedings 13.

[31] K. Nakka, H.M. Ammari, k-CSqu: ensuring connected k-coverage using cusp squares of square tessellation, J. Parallel Distrib. Comput. 182 (2023) 104749.

[32] K. Nakka, H.M. Ammari, Square tessellation for stochastic connected k-coverage in planar wireless sensor networks, in: Proceedings of the 2023 IEEE Symposium on Computers and Communications (ISCC), IEEE, 2023, pp. 864–867.

[33] wsn: A wireless sensor network simulator in python and C++ (via SWIG).AU Please provide complete details in Ref. [33]. 2023 https://github.com/darolt/wsn/.

Kalyan Nakka is a graduate student in the in the Department of Electrical Engineering and Computer Science in the Frank H. Dotterweich College of Engineering at Texas A&M University-Kingsville. He is pursuing his MS Thesis on k-coverage in planar wireless sensor networks under the supervision of Dr. Habib M. Ammari, which he started in Spring 2022. He will defend his Thesis in November 2022. He is a research assistant in Wireless Sensor and Mobile Ad-hoc Networks, Internet of Things, and Applied Cryptography Engineering (WiSeMAN-IoT-ACE) Research Lab, which is directed by Dr. Habib M. Ammari.

Habib M. Ammari is a Tenured Full Professor and the Founding Director of Wireless Sensor and Mobile Autonomous Networks (WiSeMAN) Research Lab, in the Department of Electrical Engineering and Computer Science in the Frank H. Dotterweich College of Engineering at Texas A&M University-Kingsville (TAMUK), where he joined in August 2019. He is the recipient of the Professor of the Year Award (college level award) at TAMUK in May 2023 and May 2022. Also, he received the Professor of the Year Award (college and department level award) in Computer Science at TAMUK in May 2020 and May 2021. Moreover, he is the recipient of the Outstanding Graduate Instructor Teaching Award (university level award) at TAMUK in March 2021. He served as the Graduate Computer Science Program Director from May 2020 until June 2023. He was promoted to Full Professor with tenure in the Department of Electrical Engineering and Computer Science in the Frank H.Dotterweich College of Engineering at Texas A&M University-Kingsville in November 2022. Also, he received his tenure in May 2014 in the Department of Computer and Information Science, College of Engineering and Computer Science, at the University of Michigan-Dearborn, where he served on the Distinguished Research Award Committee in 2015. Moreover, he received tenure at the Higher School of Communications in Tunis, Tunisia (Sup'Com Tunis) in 1998. He received the 2018 Albert Nelson Marquis Lifetime Achievement Award. He was selected as instructor at Stanford University in the Stanford Summer College Academy 2016 program, where he taught "Discrete Mathematical Structures: Foundational Concepts in Computer Science, Engineering, and Mathematics". He obtained his second Ph.D. degree in Computer Science and Engineering from the University of Texas at Arlington, in May 2008, and his first Ph.D. in Computer Science from the Faculty of Sciences of Tunis, in December 1996. His-main research interests lay in the area of wireless sensor and mobile ad hoc networks, including connected k-coverage, geographic forwarding, physical and information security, applied cryptography, and computational geometry in wireless sensor networks. He has a strong publication record in top-quality journals, such as ACM TOSN, ACM TAAS, IEEE TPDS, IEEE TC, Elsevier Ad Hoc Networks, Elsevier COMNET, Elsevier PMC, Elsevier JPDC, Elsevier COMCOM, and high-quality conferences, such as IEEE SECON, IEEE ICDCS, IEEE MASS, and EWSN.He published his first Springer book, "Challenges and Opportunities of Connected k-Covered Wireless Sensor Networks: From Sensor Deployment to Data Gathering" in August 2009. Also, he is the author and editor of two Springer books, "The Art of Wireless Sensor Networks: Fundamentals" and "The Art of Wireless Sensor Networks: Advanced Topics and Applications", which have been published in January 2014. In addition, he published these two current Springer books, "Mission-oriented sensor networks and systems: Art and science - Foundations" and "Mission-oriented sensor networks and systems: Art and science - Advances" in January 2019. He published his 6th Springer book, titled "Theory and Practice of Wireless Sensor Networks: Cover, Sense, and Inform", as author in December 2022. He is the recipient of the US National Science Foundation (NSF) CAREER Award in January 2011. In March 2014, he was recognized with the Distinguished Research Award at the University of Michigan-Dearborn. Furthermore, in May 2010, he was recognized with the Lawrence A. Stessin Prize for Outstanding Scholarly Publication (i.e., Distinguished Research Award) at Hofstra University. He is the recipient of the Nortel Outstanding CSE Doctoral Dissertation Award in February 2009, and the John Steven Schuchman Award for 2006– 2007 Outstanding Research by a PhD Student in February 2008. He received the Best Paper Award at EWSN in 2008, and the Best Paper Award at the IEEE PerCom 2008 Google Ph.D. Forum. He received several other prestigious awards, including the Best Graduate Student Paper Award (Nokia Budding Wireless Innovators Awards First Prize) in May 2004, the Best Graduate Student Presentation Award (Ericsson Award First Prize) in February 2004, and Laureate in Physics and Chemistry for academic years 1987 and 1988. Also, he was selected as the ACM Student Research Competition Finalist at the ACM MobiCom in September 2005. Also, he was selected for inclusion in the Marquis Who's Who in the World in 2019 and 2018, AcademicKeys Who's Who in Sciences Higher Education in 2017, Who's Who in America in 2017, AcademicKeys Who's Who in Engineering Higher Education in 2012, the AcademicKeys Who's Who in Sciences Higher Education in 2011, Feature Alumnus in the University of Texas at Arlington CSE Department's Newsletter in Spring 2011, Who's Who in America in 2010, and the 2008- 2009 Honors Edition of Madison Who's Who Among Executives and Professionals. He received several service awards, including the Certificate of Appreciation Award at MiSeNet 2014, the Certificate of Appreciation Award at 2 ACM MiSeNet 2013, the Certificate of Appreciation Award at the IEEE DCoSS 2013, the Certificate of Appreciation Award at the ACM MobiCom 2011, the Outstanding Leadership Award at the IEEE ICCCN 2011, and the Best Symposium Award at the IEEE IWCMC 2011. He is the Founding Coordinator of the Distinguished Lecture Series and the Research Colloquium Series. He was successful to invite ACM Turing Award Winners to his distinguished lecture series, such as Dr. Manuel Blum from Carnegie Mellon University, and Dr. Shafi Goldwasser from Massachusetts

Institute of Technology, who gave talks at the University of Michigan-Dearborn on January 25, 2013, and October 25, 2013, respectively, and Dr. Martin E. Hellman from Stanford University, who gave a talk at TAMUK on February 3, 2022 and also at Fordham University on October 22, 2018. He was invited to give several invited talks at reputed universities. In particular, he was invited to give a talk at the Third Arab-American Frontiers of Sensor Science Symposium, which was organized by the US National Academy of Sciences on December 5–7, 2015. Also, he served as external examiner of several Ph.D. Dissertations. He is the Founder of the Annual International Workshop on Mission-Oriented Wireless Sensor Networking (MiSeNet), which has been co-located with ACM MobiCom, IEEE INFOCOM, and IEEE MASS conferences since 2012. He served as Associate Editor of several prestigious journals, such as ACM TOSN, IEEE TC, IEEE Access, Elsevier Ad Hoc Networks, and Elsevier PMC. He serves on the Steering Committee of MiSeNet, the Annual International Conference on Distributed Computing in Sensor Systems (DCOSS), and the International Workshop on Wireless Mesh and Ad-hoc Networking (WiMAN). Moreover, he served as General Chair, Program Chair, Track Chair, Session Chair, Publicity Chair, Web Chair, and Technical Program Committee member of numerous ACM and IEEE conferences, symposia, and workshops. He is an IEEE Senior Member.